

Abstract German

Die Integration von Gruben-Wärmespeichern (Pit Thermal Energy Storage, PTES) in Hochtemperatur-Fernwärme- und -kältesysteme (District Heating and Cooling, DHC) ist durch Temperaturbeschränkungen begrenzt. In dieser Studie wird ein exergetisch basierter Bewertungsrahmen entwickelt, um Integrationsstrategien von PTES in Hochtemperatur-DHC-Netzen zu untersuchen. Zwei Konzepte werden analysiert: die Integration über Vorwärmung sowie die direkte Rückflussintegration, unterstützt durch eine Hochtemperatur-Wärmepumpe. Dynamische Simulationen werden in Modelica durchgeführt, basierend auf stündlichen Wärmelast- und meteorologischen Daten, die repräsentativ für die Schweiz sind, über einen Zeitraum von fünf Jahren. Die Ergebnisse zeigen, dass der entwickelte Rahmen Integrationsstrategien erfolgreich bewerten kann. PTES ermöglicht effektiv eine saisonale Energieverschiebung. Die Vorwärmungsintegration weist eine bessere Performance auf, während die Rückflussintegration aufgrund eines zusätzlichen elektrischen Exergieverbrauchs Nachteile zeigt. Die PTES-Vorwärmungsintegration wird daher innerhalb der definierten Systemgrenzen als eine der exergetisch effizientesten Lösungen identifiziert.

Abstract English

The integration of Pit Thermal Energy Storage (PTES) into high-temperature district heating and cooling (DHC) systems is constrained by temperature limitations. This study develops an exergy-based framework to evaluate PTES integration strategies in high-temperature DHC networks. Two concepts are analyzed: preheating integration and direct back-flow integration supported by a high-temperature heat pump. Dynamic simulations are implemented in Modelica using hourly heat demand and meteorological data representative of Switzerland over a five-year period. The results indicate that current framework can evaluate integrating strategies successfully. PTES can effectively enable seasonal energy shifting. Preheating integration achieves better performance, while back-flow integration suffers from additional electrical exergy consumption. PTES preheating integration is therefore identified as one of the more exergy-efficient solutions under the defined system boundaries.

Executive summary

The decarbonization of the heating sector represents a critical challenge in the energy transition. District heating and cooling (DHC) systems provide a promising infrastructure for integrating renewable heat sources; however, the increasing penetration of these fluctuating and low-quality heat sources has intensified the need for large-scale thermal energy storage solutions. Pit Thermal Energy Storage (PTES) has proven to be a mature and cost-effective seasonal storage technology, especially in low-temperature district heating networks. Nevertheless, its integration into existing high-temperature DHC systems remains technically challenging due to temperature limitations.

This report investigates the technical feasibility and exergetic performance of integrating PTES into high-temperature DHC networks. The primary objective is to develop a framework based on exergy analysis capable of systematically evaluating different PTES integration strategies and to quantify their impact on system performance. Two representative integration concepts are examined: (i) DHC systems with PTES preheating integration (DHC1), in which stored heat is used to preheat the return flow, and (ii) DHC systems with PTES back-flow integration (DHC2), in which stored heat is upgraded to network supply temperature using a high-temperature heat pump. A conventional high-temperature DHC system without PTES (DHC0) is used as a control case.

The assessment is conducted using a dynamic simulation model implemented in Modelica language and executed in Dymola. Hourly meteorological data and residential heat demand profiles representative of Swiss conditions are used as inputs. An exergy utilization efficiency is defined as the key performance indicator, enabling the evaluation of energy quantity and quality simultaneously. The simulations cover a five-year period to minimize the influence of initial conditions and to capture seasonal storage behavior.

The results demonstrate that:

- The developed framework and model can effectively simulate the operating states of the selected integration strategies. PTES can successfully perform seasonal energy shifting in high-temperature DHC systems by storing surplus heat during summer and supplying heat during winter.
- DHC1 exhibits the highest exergy utilization efficiency, indicating that indirect integration via return-flow preheating introduces only minor additional exergy losses.
- DHC2 shows lower performance due to the significant electrical exergy required to operate the high-temperature heat pump, even under idealized efficiency assumptions. While DHC2 reduces the exergy demand from the heat source, its total exergy consumption remains higher than that of DHC1.

Overall, the findings indicate that PTES preheating integration (DHC1) is one of the more exergy-efficient strategies for high-temperature DHC networks within the defined system boundaries. The developed exergy-based framework provides a transparent and transferable method for comparing integration concepts. Future work should focus on more detailed PTES modeling, optimized control strategies, and the inclusion of network heat losses to further improve the realism of the analysis.

Table of Contents

Executive summary.....	ii
Table of Contents.....	iii
Figures.....	iv
Tables.....	v
Abbreviations and acronyms.....	vi
1 Introduction.....	1
2 Background and theoretical research.....	2
2.1 Exergy.....	2
2.2 Systematic research.....	2
2.2.1 District Heating and Cooling System.....	2
2.2.2 Pit Thermal Energy Storage technology.....	3
2.2.3 Challenge in High temperature Integration.....	4
2.2.4 Exergy Analysis in Thermal Systems.....	5
3 Methodology.....	7
3.1 Key indicator.....	7
3.2 Boundary condition.....	7
3.2.1 DHC system without PTES (DHC 0).....	8
3.2.2 DHC system with PTES preheating integration (DHC 1).....	9
3.2.3 DHC system with PTES back-flow integration (DHC2).....	9
3.3 Calculation process and parameter assumptions.....	10
3.3.1 Reference temperature.....	10
3.3.2 Energy flow demands.....	10
3.3.3 Energy flow supply.....	11
3.3.4 Exergy factor.....	11
3.3.5 Overview of calculation process.....	12
3.4 Modelling Approach.....	12
3.4.1 Modelling Environment.....	12
3.4.2 Components in simulation.....	12
4 Evaluating Performance.....	17
4.1 Energy flow demand and reference temperature.....	17
4.2 PTES operating states.....	18
4.3 Integrating strategies performance.....	19
5 Discussion of results.....	24
6 Conclusions.....	26
6.1 Key Findings.....	26
6.2 Limitations.....	26
6.3 Recommendation.....	26
7 References.....	28
Appendix.....	30

Figures

Figure 2.1 Generic system of a district heating system (Dahash et al. 2017)	2
Figure 2.2 A classic structure of Pit thermal energy storage in Denmark (Epp, 2020)	4
Figure 3.1 Schematic defined the boundary conditions of DHC system without PTES (DHC 0)	7
Figure 3.2 Schematic defined the boundary conditions of DHC system with PTES preheating integration (DHC1)	8
Figure 3.3 Schematic defined the boundary conditions of DHC system with PTES back-flow integration (DHC2)	8
Figure 3.4 The schematic illustrating the core steps involved in calculating the key indicators is provided, with color-coded text indicating the sources of the corresponding parameters or the assumptions required.....	12
Figure 3.5 A schematic illustrating the top layer of the simulation model to be executed.....	13
Figure 3.6 Internal segments of Storage model used in simulation.....	14
Figure 3.7 A flowchart illustrating the control logic used in the simulation	15
Figure 4.1 Luzern hourly reference temperature for 2023	17
Figure 4.2 Specific hourly energy flow demand profile for 2023	18
Figure 4.3 Operating states of PTES and situation of PTES internal temperature.....	19
Figure 4.4 Operating states of PTES and situation of PTES internal temperature (With colorful highlighted)...	19
Figure 4.5 Exergy utilization efficiency of DHC1 in several different temporal resolutions	20
Figure 4.6 Exergy utilization efficiency varing of different integrating strategies with time series	21
Figure 4.7 Cumulate total exergy consumption of different integrating strategies	22
Figure 4.8 Cumulate total exergy consumption of different integrating strategies in fifth year	22

Tables

Table 1 Exergy utilization efficiency of different integrating strategies	21
Table 2 Annually cumulate total exergy consumption of different integrating	23

Abbreviations and acronyms

DHC	District heating and cooling
DHC0	DHC system without PTES
DHC1	DHC system with PTES preheating integration
DHC2	DHC system with PTES back-flow integration
HT-HP	High temperature heat pump
PTES	Pit thermal energy storage
STES	Seasonal thermal energy storage
4GDH	Fourth-generation district heating
E_{in}	Exergy input in DHC network [J]
\dot{E}_{in}	Exergy flow supply [W]
E_{uti}	Exergy demand in residential buildings [J]
\dot{E}_{uti}	Exergy flow demand [W]
P_{el}	Electricity supplied to drive high-temperature heat pump [W]
$\dot{Q}_{discharged}$	Energy transferred between PTES and DHC [W]
Q_{in}	Energy input in DHC network [J]
\dot{Q}_{in}	Energy flow supply [W]
\dot{Q}_{low}	Lower threshold of energy flow demand used in controller [W]
$\dot{Q}_{transfer}$	Energy flow transferred between the HT-HP and PTES [W]
\dot{Q}_{up}	Upper threshold of energy flow demand used in controller [W]
Q_{uti}	Energy demand in residential buildings [J]
\dot{Q}_{uti}	Energy flow demand [W]
T_{pre}	Post-preheating temperature [K]
T_r	Return temperature in pipeline after heat exchanging with demand side [K]
T_{re}	Temperature of liquid in pipeline after heat exchanging with user side [K]
T_{ref}	Reference temperature of DHC system [K]
T_s	Supply temperature to pipeline before heat exchanging with demand side [K]
T_{top}	Top segment temperature in PTES [K]
T_{2nd}	Second segment temperature in PTES [K]
\mathcal{E}_{nt}	Exergy factor when DHC exchanges heat with the heat source
\mathcal{E}_{uti}	Exergy factor when DHC exchanges heat with the user side
\mathcal{E}_{ic}	Inner coefficient of performance of HT-HP
ζ_{se}	Second-law efficiency of HT-HP
η_n	Annual exergy utilization efficiency of corresponding number strategies
$\eta_{n, T}$	Exergy utilization efficiency of corresponding number strategies in unit time

1 Introduction

Amid the escalating global challenge of carbon emissions, energy decarbonization has emerged as a critical priority. In Switzerland, residential heating accounts for a substantial share of total energy consumption, making the decarbonization of this sector particularly important. The deployment of sustainable heat sources offers significant potential for reducing heating-related carbon emissions. In this context, district heating and cooling (DHC) systems have become key enabling infrastructures for the energy transition.

With the increasing deployment of sustainable energy sources, a growing temporal mismatch has emerged between fluctuating heat source and heat required from user side. Seasonal thermal energy storage (STES) therefore plays a critical role in balancing these fluctuations. Among the available STES technologies, pit thermal energy storage (PTES) has emerged as one of the most mature and cost-effective solutions, supported by numerous practical applications and demonstrating well done performance when integrated with low-temperature DHC networks operating below 100 °C

Although PTES exhibit high suitability with DHC network, the integration of PTES into existing district heating networks remains challenging. Many established DHC systems operate at supply temperatures exceeding 100 °C, but PTES operate under standard atmospheric pressure, that means its internal temperature cannot exceed 100 °C. This temperature mismatch complicates utilization of PTES. In this situation, the direct integration between PTES and high temperature DHC network is impossible, additional components or alternative integration approaches are mandatory requirement.

To assess the theoretical compatibility of various integration strategies with high-temperature DHC networks, it is necessary to develop an analytical framework of systematically evaluating the performance of different concepts.

Furthermore, in high-temperature DHC applications, the substantial temperature disparity between the supply side and the user-side demand means that conventional energy-based analysis methods are insufficient to capture mismatches in “quality of energy” (exergy) within the system. Consequently, analytical approaches that explicitly account for variations in “quality of energy” (exergy) should be employed in the development of the analytical framework.

Accordingly, this report aims to develop a framework based on exergy analysis to evaluate the performance of different integration strategies between PTES and high-temperature DHC networks. Two representative integration strategies will be examined and comprehensively assessed by using a simulation model implemented in the Modelica language in this report.

Chapter 2 reviews the classification, operating principles, and integration challenges of DHC systems and PTES. It also introduces the fundamental concepts of exergy and summarizes relevant theoretical research on exergy analysis. Chapter 3 presents the potential integration strategies and defines the corresponding system boundaries, together with the modeling assumptions and exergy assessment methods employed in this study. Chapter 4 reports the simulation results and analyzes the exergy performance under different operating conditions. Chapter 5 discusses the implications of the results and provides a comparative evaluation of the integration strategies. Finally, Chapter 6 summarizes the main conclusions of the report and outlines directions for future research.

2 Background and theoretical research

This chapter aims to undertake a comprehensive study aligned with the stated objectives of the project. This chapter begins by introducing the fundamental concepts of exergy. The subsequent sections review existing advancements and practical applications of District Heating and Cooling (DHC) systems and Pit Thermal Energy Storage (PTES). Following this, the integration challenges between high-temperature DHC and PTES components are examined in detail. Finally, exergy-based analysis methods are presented, providing the foundation for achieving the objectives of this report.

2.1 Exergy

To examine the improvements and integration of district heating and cooling (DHC) in greater depth, it is necessary to define and clarify several fundamental concepts. This section aims to provide explanations of these basic concepts.

Exergy: The second law of thermodynamics establishes the irreversibility of processes, which gives rise to the concept of exergy. Exergy is regarded as a thermodynamic potential and can be understood as the “useful” portion of total energy (Keenan, 1941). In engineering contexts, exergy represents the potential to induce change, a concept that facilitates improved resource utilization and the mitigation of environmental impacts (Well & Gong, 2001). Exergy analysis serves as a key methodological approach in this report, and the details of exergy analysis are discussed in Section 2.24 and Chapter 3.

Quality of thermal energy: The quality of thermal energy can be expressed in terms of its exergetic content. Exergy is destroyed when energy loses quality, indicating a reduction in the efficiency of energy conversion (Dincer & Cengel, 2001).

2.2 Systematic research

2.2.1 District Heating and Cooling System

District heating and cooling systems (DHC) represent a relatively mature form of public energy infrastructure. They are designed to supply heat to residential buildings and other indoor environments with greater efficiency. A schematic representation of the conventional DHC system is provided on Fig. 2.1.

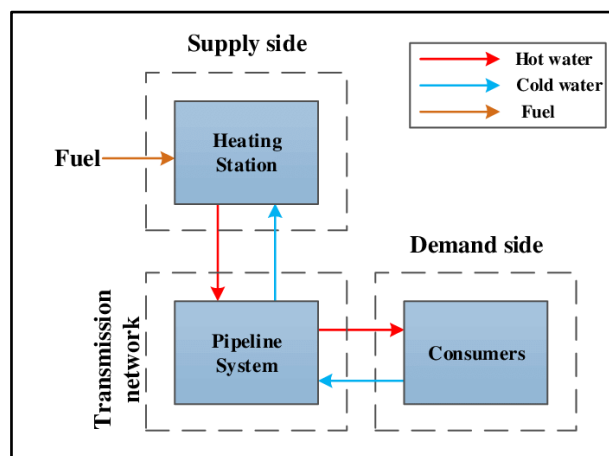


Figure 2.1 Generic system of a district heating system (Dahash et al. 2017)

In Europe, heating collectively accounts for approximately 50% of the European total final energy consumption (Muncan et al. 2024). DHC has become an appreciable quantity sector among all the heating approaches, more than 17,000 DHC systems are currently operating in Europe. This reference further contends that the development of DHC infrastructure in Europe is shifting from centralized heat supply systems (such as those relying on fossil fuel combustion and combined heat and power) to decentralized heat supply based on renewable energy sources.

At the forefront of DHC development, fourth-generation district heating (4GDH) is regarded as a feasible form for the future of district heating systems. According to Lund et al. (2014), 4GDH provides several advantages over earlier generations of DHC, including operation at lower supply temperatures (typically below 50–60 °C), the integration of intelligent control systems, and the use of renewable energy sources for heating. These features make 4GDH a suitable option for addressing future challenges such as climate change.

Muncan et al. (2024) introduce that DHC systems have been deployed in Europe for more than a century. However, a generational gap in DHC technology persists across European countries. Many existing district heating systems are still operating at relatively high supply temperatures (above 100 °C). One of the objectives of this report is to identify feasible approaches for integrating high-temperature DHC with the necessary supporting infrastructure. The following section examines the operational status of DHC systems in Switzerland and Denmark as an important research background.

DHC in Switzerland

In heating system of Switzerland, heat pumps and fossil fuel heating systems constitute the predominant heating methods, accounting for 21.3% and 54.4% respectively. DHC represents only 3.8% of the total heat supply, reflecting a marginal increase since 2000 (Federal Statistical Office, 2023). A study by Eight Advisory (2025) considered that the principal reason for the limited adoption of DHC in Switzerland is the insufficient economic benefit, which prevents it from competing cost-effectively with conventional fossil fuel heating. This limitation is likely attributable to several factors, particularly the absence of unified planning and coordination, the financial burden associated with large-scale initial investments, and Switzerland's low population density, which constrains economies of scale. Chambers et al. (2019) estimated the constitution of existing DHC in Switzerland and its potential thermal capacity through thermal atlas analysis. The study indicates that DHC serves approximately 36,000 buildings currently, corresponding to a coverage rate of 1.8%. Nevertheless, it can be inferred that DHC possesses substantial thermal potential in Switzerland. Among a series of energy-saving plan outlined by Chambers et al. (2019), increasing DHC coverage could ultimately reduce heating requires around by 40%–60%. Furthermore, the study suggests that transitioning from high-temperature DHC to lower-temperature DHC represents an important emerging trend.

DHC in Denmark

Denmark is frequently regarded as a frontrunner in DHC deployment, which had undergone rapid development in DHC since the 1970s in response to the global energy crisis. At present, approximately 55% of total heat demand in Denmark is supplied by DHC, which serves around 65% of residential building (Johansen & Werner, 2022). In addition, Denmark has widely implemented Pit Thermal Energy Storage (PTES) technology within DHC, primarily to address energy fluctuations arising from the large-scale solar thermal sector. These two mature technologies operate in strong complementarity in the Danish context (Bolton et al., 2023).

Despite DHC system in Denmark is maturity, Johansen and Werner (2022) emphasize that the sector continues to face significant challenges. A central issue is the transition from combustion-based to non-combustion energy sources. Future DHC is expected to increasingly rely on alternatives such as large-scale electric heat pumps, solar thermal collectors, industrial waste heat, and geothermal energy. This transformation introduces not only technical but also policy and investment challenges, necessitating new infrastructure and market frameworks. Furthermore, the growing competition from household heat pumps represents an additional challenge. In low-density residential areas, household heat pumps are becoming increasingly cost-effective and appealing, potentially reducing the market share of DHC in such regions.

2.2.2 Pit Thermal Energy Storage technology

Pit thermal energy storage (PTES) represents one of several forms of seasonal thermal energy storage technologies. Its fundamental concept is to enhance the efficient utilization of generated energy through storage in large-scale pits. PTES is frequently employed to mitigate peak loads in DHC systems, particularly those arising from seasonal demand fluctuations (Sveinbjörnsson et al. 2019).

The key technical components of PTES include geometry design, inlet and outlet configuration, cover construction, insulation materials, and liner materials (Xiang et al., 2022). A typical PTES structure takes the form of an inverted pyramid with a rectangular cross-section, as illustrated in Figure 2.2. This design seeks to achieve a balance between high structural stability and relatively low construction costs for thermal storage applications (Xiang et al., 2022). Water is commonly used as the thermal storage medium in PTES due to its high specific heat capacity and widespread availability.

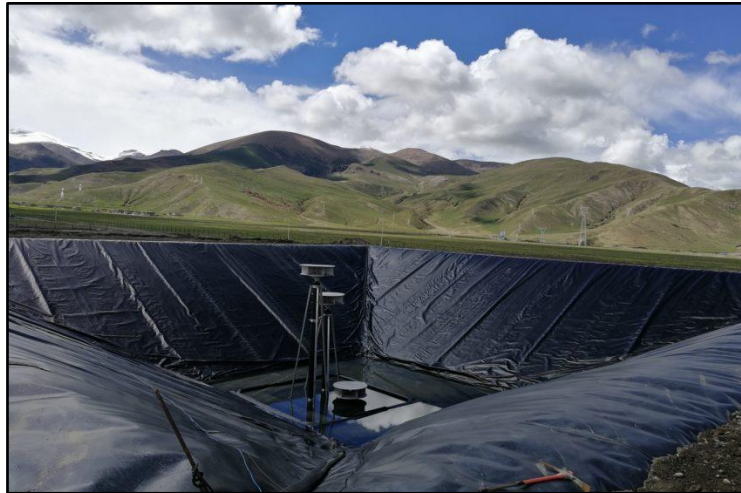


Figure 2.2 A classic structure of Pit thermal energy storage in Denmark (Epp, 2020)

Thermal loss in PTES

Minimizing heat loss in energy storage systems constitutes a critical challenge. Sveinbjörnsson et al. (2019) contend that low specific heat losses of large-scale TES represent a key advantage. This Reference also considers that thermal loss is determined by two metrics primarily: the surface-to-volume ratio of the storage capacity and the quality of the insulation material employed. In typical PTES applications, polymer liners are used as the primary insulation material. These materials exhibit a lifetime of approximately 18–25 years when operated at storage temperatures below 70 °C; however, operation at higher temperatures will markedly reduce their durability (Xiang et al. 2022). This poses a challenge for the effective integration of PTES into high-temperature DHC.

Dahash et al. (2019) suggest that effective thermal stratification can also be another indicator in reducing thermal losses in PTES, whereas excessive mixing diminishes the usable storage temperature. To mitigate this effect, it is essential to ensure that water flows at the inlet and outlet does not generate excessive turbulence.

Gao et al. (2022) conducted a series of measurements and simulations about the heat loss in a constructed PTES in Denmark over a five-year period. The PTES had a storage capacity around 60,000 m³. Results concluded that the system achieves a thermal efficiency of approximately 90.1% and average annual thermal loss is 1,157 MWh.

Economics of scale of PTES

PTES exhibits pronounced economies of scale, as larger storage capacities can substantially reduce the cost per cubic meter (Sveinbjörnsson et al., 2019). Several large-scale PTES facilities in Denmark have achieved costs as low as 20 €/m³. Moreover, Sifnaios et al. (2025), in an analysis of PTES integration with high-temperature DHC in a Danish city, concluded that employing lower charge temperatures in PTES enhances the coefficient of performance of heat pumps, thereby further reducing overall PTES costs.

2.2.3 Challenge in High temperature Integration

High-temperature DHC systems (operating above 100 °C) had a substantial share of the overall DHC infrastructure. However, their integration with various components exists significant challenges.

Xiang et al. (2022) found that the long-term use of common insulated materials (high-density polyethylene and polypropylene) in PTES at a standard temperature of 90 °C will significantly reduce the lifetime of these materials. The need for frequent liner replacement consequently increases the cost of PTES integration. Sifnaios and Jensen (2023) sought to extend the lifespan of insulation by increasing the thickness of polypropylene (PP) liners to 2.5 mm in a short-term high-temperature PTES installation. Their study estimated that these modified liners could achieve a service life of up to 50 years at operating temperatures of 95 °C.

Another challenge in integrating PTES with high-temperature DHC using conventional methods is that PTES operates at standard atmospheric pressure over whole life period, which limits the stored water temperature to 100 °C. This is incompatible with the supply temperatures exceeding 100 °C required by high-temperature DHC systems. Consequently, the development of technically feasible integration strategies between PTES and high-temperature DHC constitutes one of the primary objectives of this report.

The integration of high-temperature DHC systems with household heating also remains a significant challenge. Typical residential heating requirements generally do not exceed 65 °C, while systems such as floor heating often operate at even lower supply temperatures (Jangsten et al., 2017). Supplying such low-temperature demand with high-temperature DHC is considered inefficient, as it results in exergy destruction due to the temperature mismatch (Gong & Werner, 2015). Moreover, the literature indicates that the efficiency of DHC systems is more accurately assessed through measurements of exergy destruction within the network. Methods for exergy analysis are outlined in Section 2.2.4.

Furthermore, with the global trend toward decarbonization, renewable heat sources such as solar thermal, biomass thermal, and thermal by waste incineration are gaining increasing prominence. A common characteristic of these decentralized heat sources is their low heat quality. Integrating high-temperature DHC with such low-quality heat sources presents notable challenges, as the connection requires additional heat quality enhancement processes, such as heat pumps (Muncan et al. 2024).

2.2.4 Exergy Analysis in Thermal Systems

Comparing energy demand of DHC system with energy supply of DHC system directly is a common and intuitive assessment approach to evaluate the performance of system. However, it does not accurately capture the mismatch of quality between them. With the continued advancement of renewable energy sources and the global trend toward decarbonization, the alignment of heat quality has become a critical issue.

Gong & Werner (2015) introduced the concept of exergy analysis into the assessment of DHC efficiency. They argue that low-quality heat is sufficient to meet demands in residential buildings, such as space heating and domestic hot water. High-temperature DHC is inherently inefficient due to substantial exergy destruction. This reference defines the exergy factor ε as a key indicator for evaluating DHC systems, where ε represents the ratio of exergy input to heat input.

The relationship of exergy factor ε_{nt} in DHC network can be given by:

$$\varepsilon_{nt} = \frac{E_{in}}{Q_{in}} \quad (1)$$

Where:

E_{in} is the exergy input in DHC network [J]

Q_{in} is the energy input in DHC network [J]

Well & Gong (2001) derived the expression for ε in a one-pipe system. In a two-pipe DHC system, only a portion of the supplied heat is utilized by the consumer. That can be considered as the return water temperature remains above the reference temperature. Consequently, the relationship between the supply temperature T_s and the return temperature T_r must be considered in such cases (Gong & Werner, 2015).

The exergy factor ε_{nt} in DHC network can be given by:

$$\varepsilon_{nt} = 1 - \frac{T_{ref}}{T_s - T_r} \ln \frac{T_s}{T_r} \quad (2)$$

Where:

T_{ref} is the reference temperature of DHC system [K]

T_r is the return temperature in pipeline after heat exchanging with demand side [K]

T_s is the supply temperature in pipeline before heat exchanging with demand side [K]

Based on calculations using typical pipeline temperatures, a decrease in DHC pipeline temperature leads to a corresponding reduction in the exergy factor of the entire system, indicating that the DHC network delivers less exergy. This also reflects the technological improvement of DHC systems. The exergy factor of a typical high-temperature DHC is approximately 24%, whereas that of a low-temperature DHC can decrease to around 9% (Gong & Werner, 2015).

In addition, Gong & Werner (2015) defined the exergy utilization efficiency to represent the degree of correspondence between the DHC network and the heat demand of residential buildings. The exergy utilization efficiency η denotes the proportion of total exergy input that is required to satisfy exergy demand of residential buildings.

The exergy utilization efficiency η can be given by:

$$\eta = \frac{E_{uti}}{E_{in}} = \frac{Q_{uti} \varepsilon_{uti}}{Q_{in} \varepsilon_{nt}} \quad (3)$$

Where:

E_{uti} is the exergy demand in residential buildings [J]

Q_{uti} is the energy demand in residential buildings [J]

ε_{uti} is the exergy factor when DHC exchanges heat with the user side

ε_{in} is the exergy factor when DHC exchanges heat with the heat source

3 Methodology

This chapter aims to examine technically feasible integration strategies for incorporating PTES into existing high-temperature DHC systems and to develop a theoretical exergy analysis framework capable of effectively highlighting the performance of DHC systems. This chapter will also discuss the simulation environment and modeling details involved in implementing the exergy analysis framework. The preceding sections present two technically feasible integration strategies and specify their corresponding system boundaries. Subsequently, the following sections define the sources of several key parameters as well as the assumptions or calculation methods applied. Finally, this chapter provides a comprehensive description of the simulation environment used in this report and introduces the key components of the implemented model, including the control component, the PTES with optional HT-HP, and the calculation component.

3.1 Key indicator

The exergy utilization efficiency η is employed in this report as a key indicator for evaluating the efficiency performance of the DHC system achieved through PTES integration. It can be interpreted as the proportion of the total exergy supplied by the system that is effectively utilized at the user side, it can be expressed as follows:

$$\eta = \frac{\text{Utilized part of exergy in system}}{\text{Total exergy input in system}}$$

Exergy utilization efficiency η is a dimensionless coefficient ranging from 0 to 1. A higher value of η indicates lower exergy losses during the operation of the DHC, thereby reflecting superior system performance.

3.2 Boundary condition

This report aims to investigate the potential of PTES to enhance the efficiency of high-temperature DHCs through exergy analysis. Accordingly, the definition of system boundaries within the exergy framework is essential. As illustrated in Figure 2.1, Dahash et al. (2017) present a generic DHC system based on mass flow. This report will build upon a new framework by refining and redefining the system boundaries.

To minimize assumptions involving excessive uncertainty, this report employs exergy flow as the analytical framework and energy flow as the system control logic. The system boundaries are defined for two different integration strategies: DHC system with PTES preheating integration (**DHC1**), DHC system with PTES back-flow integration (**DHC2**). In addition, DHC system without PTES (**DHC 0**) will be simulated as a control group to evaluate the system performance shown through various integration strategies. All the systems are shown in following diagrams.

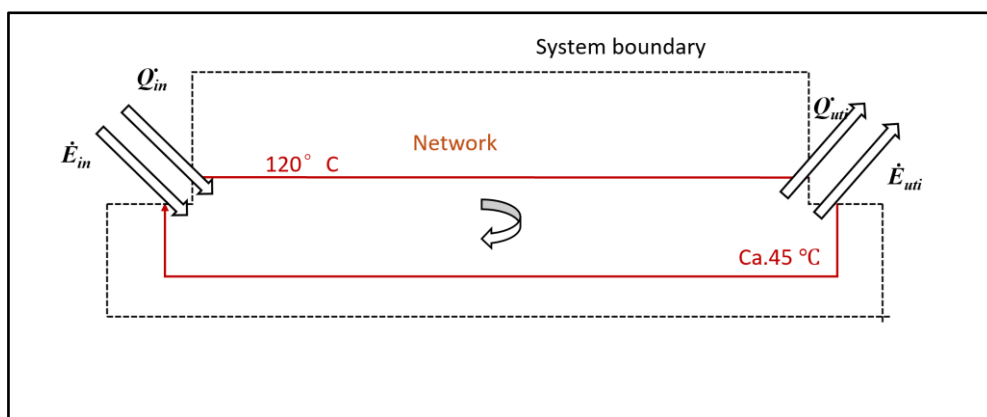


Figure 3.1 Schematic defined the boundary conditions of DHC system without PTES (**DHC 0**)

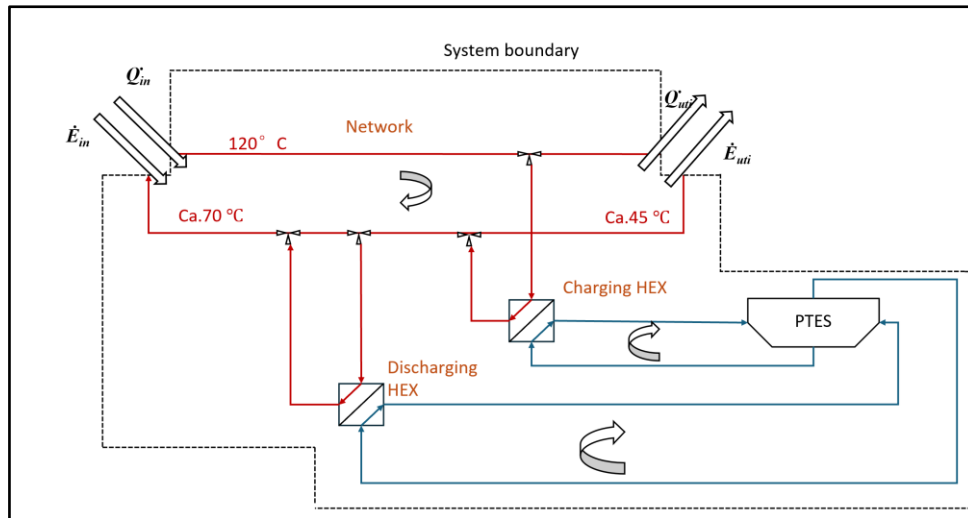


Figure 3.2 Schematic defined the boundary conditions of DHC system with PTES preheating integration (**DHC1**)

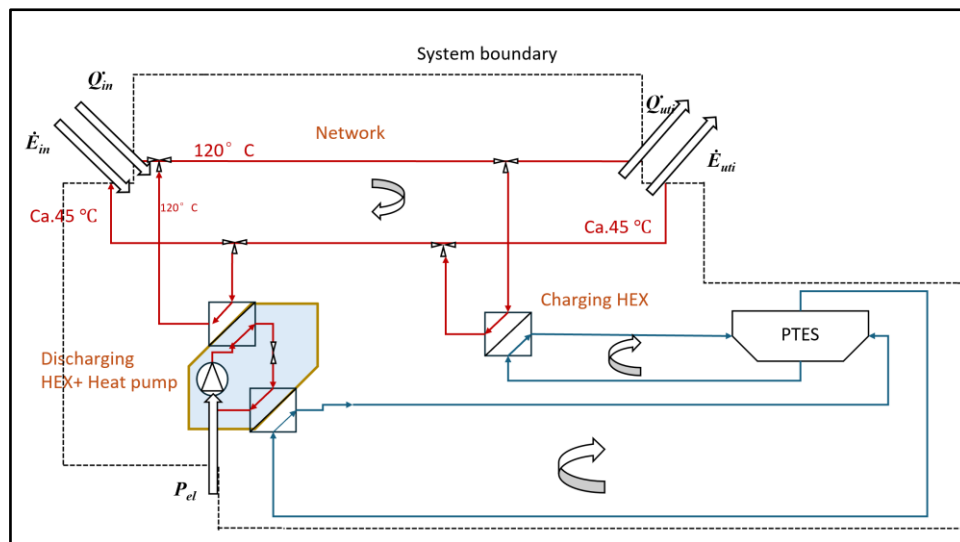


Figure 3.3 Schematic defined the boundary conditions of DHC system with PTES back-flow integration (**DHC2**)

Figures 3.1, 3.2, and 3.3 illustrate the schematics of all systems considered in the simulations. These schematics emphasize the components within the defined system boundaries while excluding those outside the system scope. In addition, they depict the energy transfer processes between the system and its surrounding environment. It is important to note that the system boundaries do not encompass the heat exchangers located at the heat source and user sides. This exclusion is based on the principles of energy flow analysis, whereby the heat exchangers are regarded as integral parts of the heat source distribution network and the user distribution network respectively. Additional design diagrams related to the integration strategies are provided in Appendix A, including overview and black-box representations.

3.2.1 DHC system without PTES (DHC 0)

Figure 3.1 illustrates the system boundary of a DHC system without PTES (hereinafter referred to as **DHC0**). DHC0 includes the entire delivery network except for the heat exchangers at the heat source and user sides. The energy exchange between the system and the environment is characterized by the following parameters in DHC0: energy flow supply \dot{Q}_{in} , energy flow demand \dot{Q}_{uti} , exergy flow supply \dot{E}_{in} , and exergy flow demand \dot{E}_{uti} .

The exergy utilization efficiency η_0 of DHC0 can be determined by substituting all exergy terms in Equation 2 with the corresponding exergy flow terms. The exergy factor within the network ε_{in} and the exergy factor within the user distribution network ε_{uti} , will be discussed in Section 3.3.4 along with the corresponding methodology.

The exergy utilization efficiency $\eta_{0,T}$ of DHC0 can be determined by:

$$\eta_{0,T} = \frac{\dot{E}_{uti}}{\dot{E}_{in}} = \frac{\dot{Q}_{uti}\varepsilon_{uti}}{\dot{Q}_{in}\varepsilon_{in}} \quad (3)$$

Where:

\dot{E}_{in} is the exergy flow supply [W]

\dot{E}_{uti} is the exergy flow demand [W]

\dot{Q}_{in} is the energy flow supply [W]

\dot{Q}_{uti} is the energy flow demand [W]

ε_{uti} is the exergy factor when DHC exchanges heat with the user side

ε_{in} is the exergy factor when DHC exchanges heat with the heat source

The simulation period in this report spans five full years, and the temporal resolution is hourly, this will be further discussed in Section 3.3. The annual exergy utilization efficiency should be calculated for each DHC. The annual exergy utilization efficiency η_0 of DHC0 can be expressed as follows:

$$\eta_0 = \frac{\int \dot{E}_{uti} dt}{\int \dot{E}_{in} dt} \quad (4)$$

3.2.2 DHC system with PTES preheating integration (DHC 1)

Figure 3.2 illustrates the system boundary of DHC system with PTES preheating integration (hereinafter referred to as **DHC1**). DHC1 represents one feasible configuration for PTES integration. This strategy seeks to avoid direct integration by utilizing heated reflow. In this design, the PTES are not required to raise the return flow temperature to the supply level of approximately 120 °C. Instead that it serves to preheat the return flow, thereby reducing the energy demand placed on the heat source. In the DHC1 design, the system boundary encompasses not only the entire network but also the entire PTES. This configuration implies that the PTES operates without any direct interaction or exchange with the external environment.

The exergy utilization efficiency $\eta_{1,T}$ of DHC1 and annual exergy utilization efficiency η_1 of DHC1 can also be expressed using Equation 3 and 4, because the defined system boundary does not introduce any additional energy or mass exchange between the system and the environment.

3.2.3 DHC system with PTES back-flow integration (DHC2)

Figure 3.3 illustrates the system boundary of DHC system with PTES back-flow integration (hereinafter referred to as **DHC2**). In DHC2, the PTES directly merges the heated water flow with the flow supplied in DHC network. This design incorporates a high-temperature heat pump as an auxiliary component. The function of the high-temperature heat pump is to elevate the energy flow charged by the PTES to the standard supply temperature of the DHC network pipeline, thereby enabling the direct integration of the PTES with the DHC. In addition to the four parameters previously described the energy exchange in DHC2 must also account for the additional electrical power P_{el} required to operate the high-temperature heat pump. The exergy utilization efficiency $\eta_{2,T}$ of DHC2 can be expressed using Equation 5.

$$\eta_{2,T} = \frac{\dot{E}_{uti}}{\dot{E}_{in} + P_{el}} \quad (5)$$

Where:

P_{el} is electricity supplied to drive high-temperature heat pump [W]

The annual exergy utilization efficiency η_2 of DHC2 can be expressed using Equation 6.

$$\eta_2 = \frac{\int \dot{E}_{uti} dt}{\int \dot{E}_{in} dt + \int P_{el} dt} \quad (6)$$

3.3 Calculation process and parameter assumptions

This section outlines the calculation process required to determine the key indicator of this report. The methods used to obtain the parameters required for the calculations and the necessary data series will be presented in the following sections.

3.3.1 Reference temperature

Determining the ambient temperature is essential, as it fundamentally influences the performance of the entire system. Pons (2009) argues that the ambient temperature should be defined as a constant value to ensure energy conservation under reversible conditions. This approach enables the results to represent the maximum achievable work potential of the system. Torío and Schmidt (2010) argue that exergy and exergy efficiency of system should exhibit sensitivity to the ambient temperature, implying that the reference temperature should closely reflect the actual outdoor conditions. However, because the outdoor environment is inherently dynamic and varies over time, only a dynamic reference temperature can accurately capture system performance. This report aims to simulate a real DHC system to evaluate its exergy utilization efficiency, which requires adopting a non-ideal model. Furthermore, because the heat demand on the user side is strongly correlated with the dynamic outdoor temperature, a reference temperature that varies in accordance with the heat demand profile is necessary. For these reasons, a dynamic reference temperature is employed in this report.

The raw meteorological data used in this report consists of hourly measurements from 00:00 on 1 January 2023 to 23:00 on 31 December 2023 (MeteoSchweiz, 2025). These data were recorded at the Luzern meteorological station. The use of hourly dynamic data is considered appropriate, as this temporal resolution aligns well with the corresponding energy flow demand data.

Furthermore, because hourly temperatures exhibit substantial short-term fluctuations. This report also calculates the weekly, monthly, and annually average temperature using the same meteorological data and conducts corresponding simulations for comparative analysis.

3.3.2 Energy flow demands

Energy flow demand \dot{Q}_{uti} can be regarded as the total heat demand of a residence connected to the DHC. \dot{Q}_{uti} also encompasses potential losses associated with appliances or with the heat distribution network within the residence. This report adopts an existing user-side thermal demand profile from previous projects as the energy flow demand input for the simulation. This data profile provides the annual heat demand of connected DHC users in a Swiss context, with an hourly temporal resolution. This level of detail effectively captures variations in energy flow demand across both diurnal and seasonal timescales.

3.3.3 Energy flow supply

The energy flow supply \dot{Q}_{in} is dependent on the energy flow demand \dot{Q}_{uti} and the energy flow discharged $\dot{Q}_{discharge}$. The value of \dot{Q}_{in} can therefore be calculated using the expression given in Equation 7. This relationship reflects the conservation of energy within the system in accordance with the first law of thermodynamics. \dot{Q}_{uti} is generally assigned a negative value, as it represents energy leaving the system. $\dot{Q}_{discharge}$ denotes the charging or discharging process of the PTES within the DHC network, where charging is treated as a negative value and discharging as a positive value.

The energy flow supply can be calculated by:

$$\dot{Q}_{in} + \dot{Q}_{uti} + \dot{Q}_{discharge} = 0 \quad (7)$$

Where:

$\dot{Q}_{discharge}$ is the energy transferred between PTES and DHC [W]

$\dot{Q}_{discharge}$ is computed in real time using the logic components implemented in the simulation to control the interaction between the PTES and the DHC network. Further details regarding this control mechanism are provided in Section 3.4.3.

3.3.4 Exergy factor

The exergy factor represents the proportion of the corresponding energy flow that is converted into exergy flow in the existing system. It can be represented in equation 1 shown in section 2.2.4

Equation 2 illustrates the method for calculating the exergy factor supplied by the network ε_{in} and the exergy factor extracted from the user distribution network ε_{uti} . To apply this calculation, reasonable assumptions must be made regarding the supply and return temperatures of the DHC system. A supply temperature of 120 °C is considered appropriate for high-temperature network operation, representing the temperature of the mass flow after being pressurized above standard atmospheric pressure. The return temperature of the DHC network is assumed to be a constant value, which can be practically maintained by regulating the mass flow within the corresponding pipelines. In a simulation based on energy flow, adopting a constant return temperature simplifies the system complexity and focuses on variations in energy and exergy.

The return temperature T_{re} for both the control group DHC0 and the integration strategy DHC2 is assumed to be 50 °C. In contrast, the integration strategy DHC1 incorporates a reflux preheating process. Therefore, it can be calculated using the assumed return temperature together with the corresponding mass flow when calculating the post-preheating temperature.

The post-preheating temperature T_{pre} can be calculated as:

$$T_{pre} = (T_r - T_s) \frac{\dot{Q}_{discharge}}{\dot{Q}_{uti}} + T_{re} \quad (8)$$

Where:

T_r is temperature of liquid in pipeline after heat exchanging with user side [K]

T_s is temperature of liquid in pipeline after heat exchanging with heat source [K]

It is worth noting that when calculating the exergy factor for the exergy flow demand, the supply and return temperatures on the DHC side should be used rather than the corresponding temperatures within distribution

network in user side. This is because the system boundary accounts for the interaction between the DHC network and the environment and does not include the distribution network on the user side.

3.3.5 Overview of calculation process

Figure 3.4 illustrates the core methodology used in this report to evaluate the performance of different integration strategies. The key indicators derived from this methodology will be presented in the results section in the form of integrals and corresponding visual charts

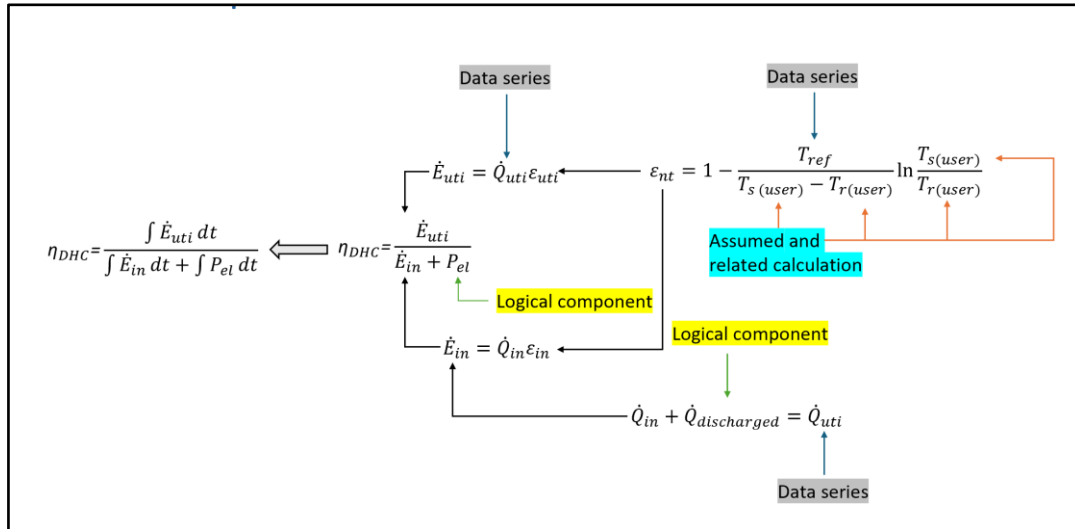


Figure 3.4 The schematic illustrating the core steps involved in calculating the key indicators is provided, with color-coded text indicating the sources of the corresponding parameters or the assumptions required.

3.4 Modelling Approach

3.4.1 Modelling Environment

The simulations presented in this report were conducted using Dymola 2023 and implemented in the Modelica programming language. The “Modelica Standard Library (MSL)” was used for fundamental components such as prescribed heat or exergy flows and sensors, while the “Buildings Library” was employed for thermohydraulic components including sinks and storage units.

3.4.2 Components in simulation

Figure 3.5 presents the top layer schematic of the DHC simulation conducted in this report. The two numerical inputs to the model: the reference temperature and the heat flow demand. These numerical inputs are derived from meteorological data and the heat demand profile respectively. All inputs are processed as signals through the control component, the PTES with optional HT-HP, as well as the calculation component, which collectively perform regulation, feedback, and computational tasks to generate the final outputs. These outputs include the key performance indicators of the system, such as energy utilization efficiency and total energy supply. In the top layer schematic, the three major components are consolidated into corresponding black boxes to enhance the clarity of the system representation.

The control component implements the control logic described in Section 3.4.3. Its primary function is to regulate the operating state of the PTES in real time and to determine the required charging or discharging energy.

The PTES with an optional HT-HP serves as the integrated energy storage component within the DHC system. Its primary function is to provide feedback on the internal temperatures of the PTES to the control component, thereby enabling real-time operational judgements by the controller. In addition, an additional high-temperature heat pump must be included in the model to account for its electrical power consumption when simulating the integrating strategy DHC2 described in following context.

The Calculation component receives all inputs from the other components and incorporates an internal pipeline temperature computation mechanism. Its primary function is to aggregate all parameter values and compute the exergy-related results corresponding to the current input conditions.

The simulation period was set to 5 years with the same data profile repeated annually. This duration was chosen to minimize the influence of initial conditions (such as the initial internal temperature of the PTES) on the results. Detailed information regarding the Dymola simulation program is provided in Appendix B.

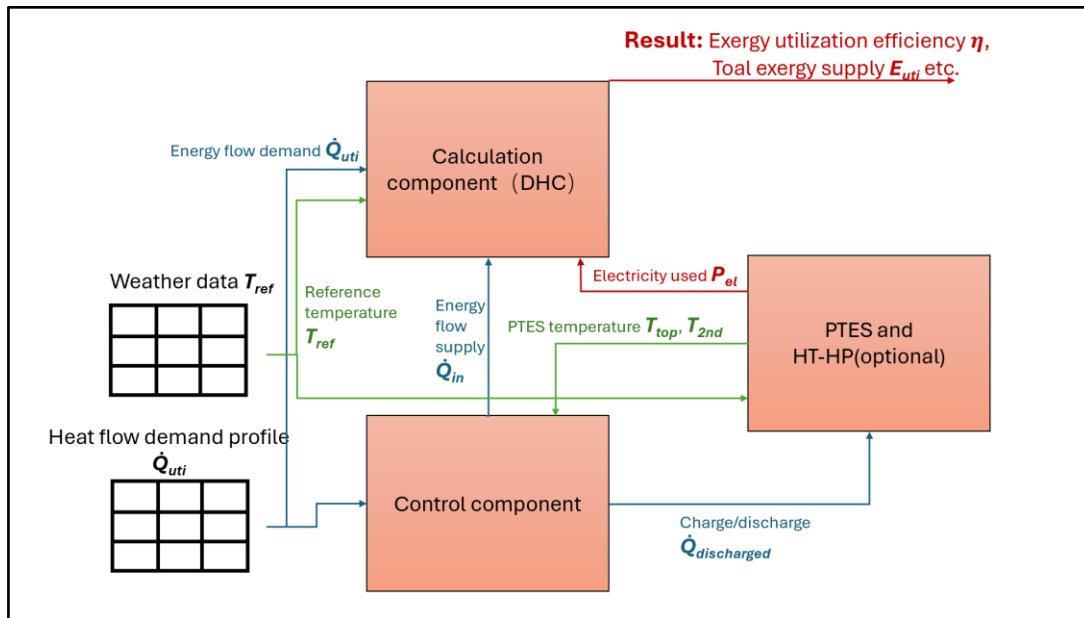


Figure 3.5 A schematic illustrating the top layer of the simulation model to be executed.

PTES component

The simulation model employed in this report utilizes an existing stratified storage model (Fluid.Storage.Stratified) from the “Buildings” Library. In this model, the internal temperature of the storage unit is adjusted through the input heat flow $Q_{discharge}$. This process is additionally influenced by a reference temperature T_{ref} , which is therefore included as a required input. The total storage volume is set to 400,000 m³, and the model represents the storage medium using multiple temperature segments. Based on the temperature stratification and heat transfer characteristics of the storage model, this report adopts the top segment temperature T_{top} and the second segment temperature T_{2nd} as the monitored range by the controller to control the operating states of the PTES.

It should be noted that this storage model is a general-purpose representation and cannot fully capture the specific physical characteristics of a PTES, such as the surrounding soil properties or the detailed geometry of the storage pit. However, by adjusting the heat transfer parameters within the model, the resulting simulation inaccuracies can be partially mitigated.

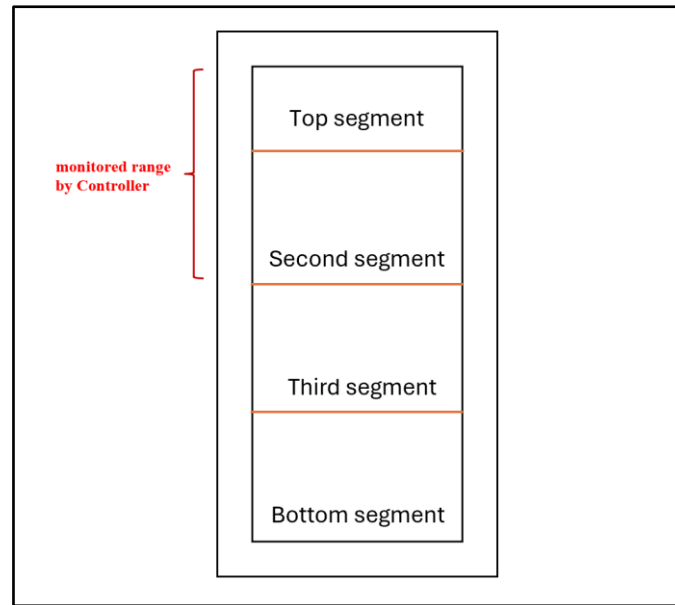


Figure 3.6 Internal segments of Storage model used in simulation

Logic controller

The core concept underlying the PTES simulation logic in this report is peak shifting. This principle is consistent with the emerging heating paradigm that integrates a variety of sustainable heat sources. The objective is to charge the PTES by supplying excess energy to the DHC network during periods of high sustainable heat-source availability (summer) and subsequently discharge the stored energy during periods of low availability (winter), thereby mitigating potential deficits in sustainable energy supply.

Figure 3.7 presents the logic-control flowchart used in the simulation. This control mechanism requires three input variables: the energy flow demand \dot{Q}_{uti} , the top segment temperature of the PTES T_{top} , and the second segment temperature of the PTES T_{2nd} . Both T_{top} and T_{2nd} serve as feedback signals influenced by $\dot{Q}_{discharged}$. The controller applies two levels of decision-making.

The first decision determines whether the system should charge or discharge the PTES for a given data point. To perform this assessment, two energy thresholds are defined: the upper threshold of energy flow demand \dot{Q}_{up} and the lower threshold \dot{Q}_{low} . The value of \dot{Q}_{up} corresponds to the 70th percentile of the data profile discussed in Section 3.3.2, while \dot{Q}_{low} corresponds to the 35th percentile.

The second decision assesses whether the PTES can charge or discharge, ensuring that the internal PTES temperature does not exceed or fall below acceptable operational limits. In the simulation, the PTES temperature is regulated such that the top segment temperature does not exceed 90 °C and the second segment temperature does not fall below 60 °C.

PTES has four potential operating states, which are:

Charging to top segment: The DHC network charges the top segment of the PTES when \dot{Q}_{uti} exceeds the upper threshold and top segment temperature of the PTES remains below 90 °C.

Charging to second segment: The DHC network charges the second segment of the PTES when \dot{Q}_{uti} exceeds the upper threshold and top segment temperature of the PTES remains below 90 °C. It is worth noting that in the actual simulations, T_{2nd} rarely reaches high temperatures. Therefore, the controller disregards the condition in which T_{2nd} approaches high values (e.g. 90 °C).

Discharging: PTES will discharge energy to the DHC network when \dot{Q}_{uti} is lower compared than lower threshold and second segment temperature of PTES remain over 60 °C.

Idle: In all remaining cases, the PTES remains idle, meaning that no charging or discharging occurs. Under this operating state, the system can be regarded as equivalent to DHC0.

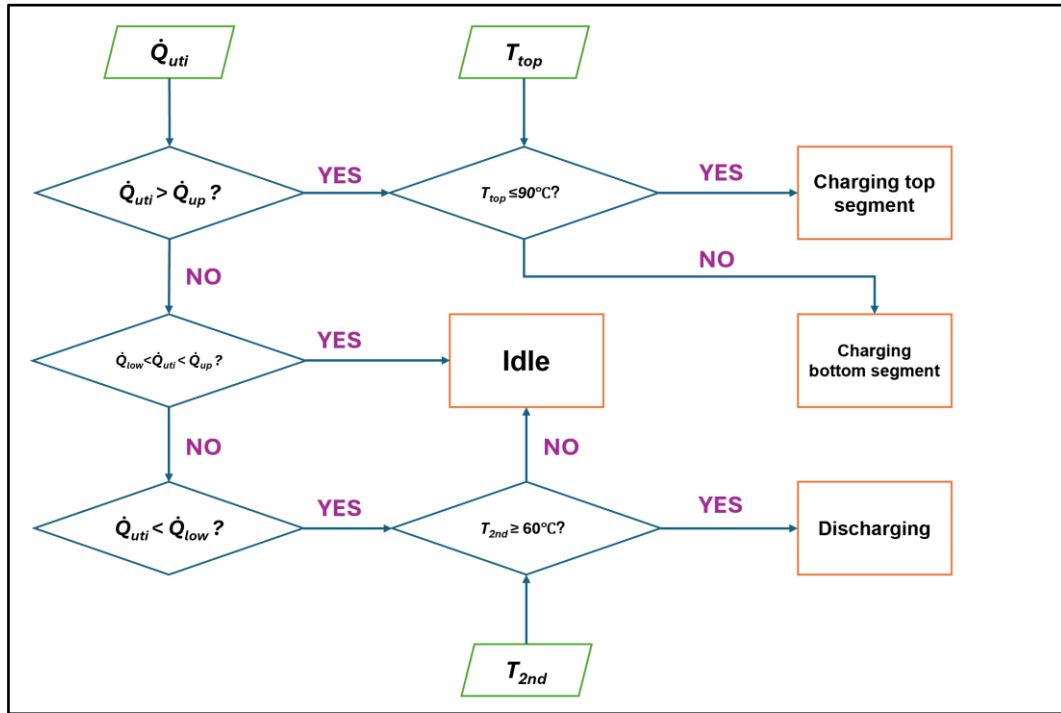


Figure 3.7 A flowchart illustrating the control logic used in the simulation

High temperature Heat pump

The simulation model of DHC2 incorporates a corresponding high-temperature heat pump. Within the simulation, the HT-HP component is designed to decompose the controller-provided heat flow $\dot{Q}_{discharged}$ into the electrical power consumption P_{el} required to drive the heat pump and the thermal energy flow $\dot{Q}_{transfer}$ exchanged between the heat pump and the PTES. The relationship among these three parameters is defined by Equation 9

$$\dot{Q}_{discharged} = P_{el} + \dot{Q}_{transfer} \quad (9)$$

Where:

$\dot{Q}_{transfer}$ is the energy flow transferred between the HT-HP and PTES [W]

The electrical power consumption of HT-HP is influenced by its inner coefficient of performance and second-law efficiency. Moreover, since the HT-HP operates only when the PTES is in a discharging state, the electrical power consumption satisfies $P_{el} = 0$ when $\dot{Q}_{discharge} \leq 0$. When $\dot{Q}_{discharge} > 0$, the value of P_{el} is determined according to Equation 10.

$$P_{el} = \frac{\dot{Q}_{discharged}}{\zeta_{se} \varepsilon_{ic}} \quad (10)$$

Where:

ζ_{se} The second-law efficiency of HT-HP

ϵ_{ic} The inner coefficient of performance of HT-HP

To assess the influence of idealized versus realistic HT-HP performance on the results of DHC2, the HT-HP component in the simulation model was evaluated under two conditions: an ideal case with a second-law efficiency of 1 and a realistic case with a second-law efficiency of 0.5. The results obtained from these two scenarios were subsequently compared.

The inner coefficient of performance of HT-HP can be calculated using Equation 11. It should be noted that the two temperatures used in this equation require the assumption of an additional temperature difference relative to the ambience temperature of the heat pump. In the simulations conducted in this report, a temperature difference of 5 K was adopted.

$$\epsilon_{ic} = \frac{(T_s + 5)}{(T_s + 5) - (T_{2nd} - 5)} \quad (11)$$

4 Evaluating Performance

This chapter discusses the simulation results obtained using the methodology described in Chapter 3. The results are examined through a combination of visualizations and summary tables. The first section introduces and explains two key data profile inputs used in the simulations. The subsequent sections analyze the operating states of the PTES under the implemented control logic. Finally, the chapter evaluates and compares the related performance indicators of the control group DHC0, integration strategies DHC1 and DHC2 under various configurations.

4.1 Energy flow demand and reference temperature

This section discusses two parameters that serve as inputs to the simulation model, as introduced in Sections 3.3.1 and 3.3.2. Figure 4.1 provides a visualization of the reference temperature data profile for one year duration. The ambient temperature, which serves as the reference temperature, exhibits a pronounced seasonal variation between winter and summer. The warmest period of the year occurs primarily between June and August, whereas the coldest periods are concentrated in January, February, and December, with the annual minimum typically occurring in February. Moreover, Figure 4.1 indicates that temperature fluctuations are more pronounced during the summer months.

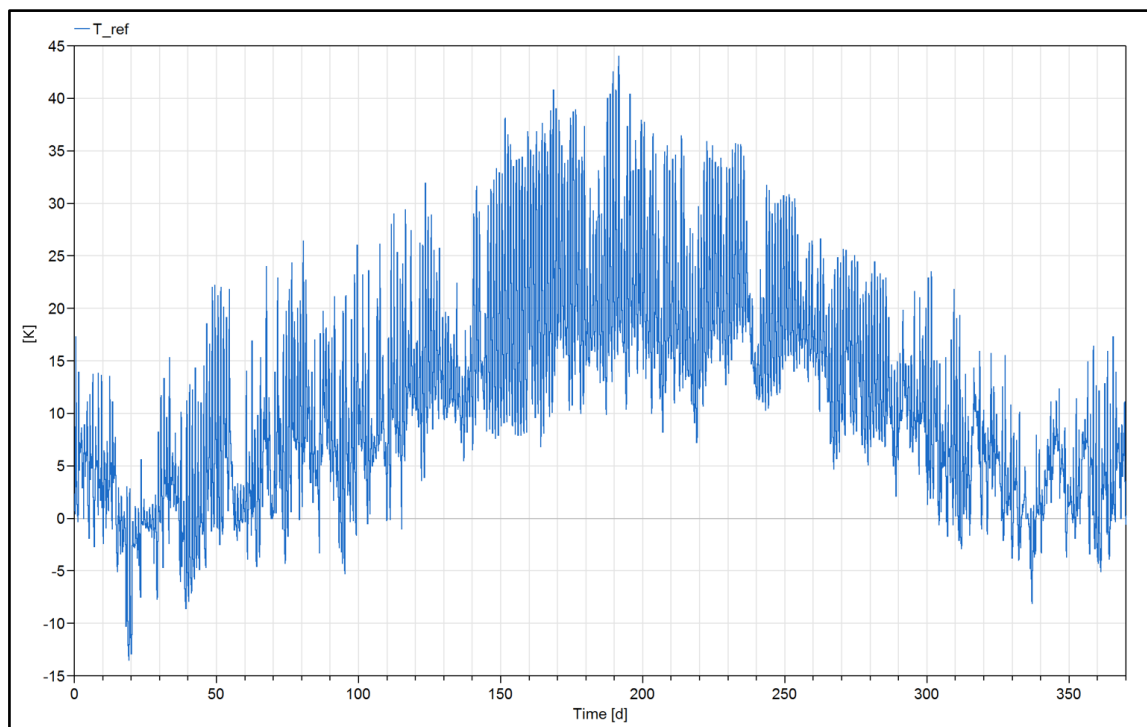


Figure 4.1 Luzern hourly reference temperature for 2023

Figure 4.2 presents the heat demand profile employed in previous studies. This visualization illustrates the total hourly residential energy flow demand at the specified rates. As shown in Figures 4.1 and 4.2, the energy flow demand exhibits a clear correlation with the reference temperature. Overall demand is lower during the summer months and higher during the winter period.

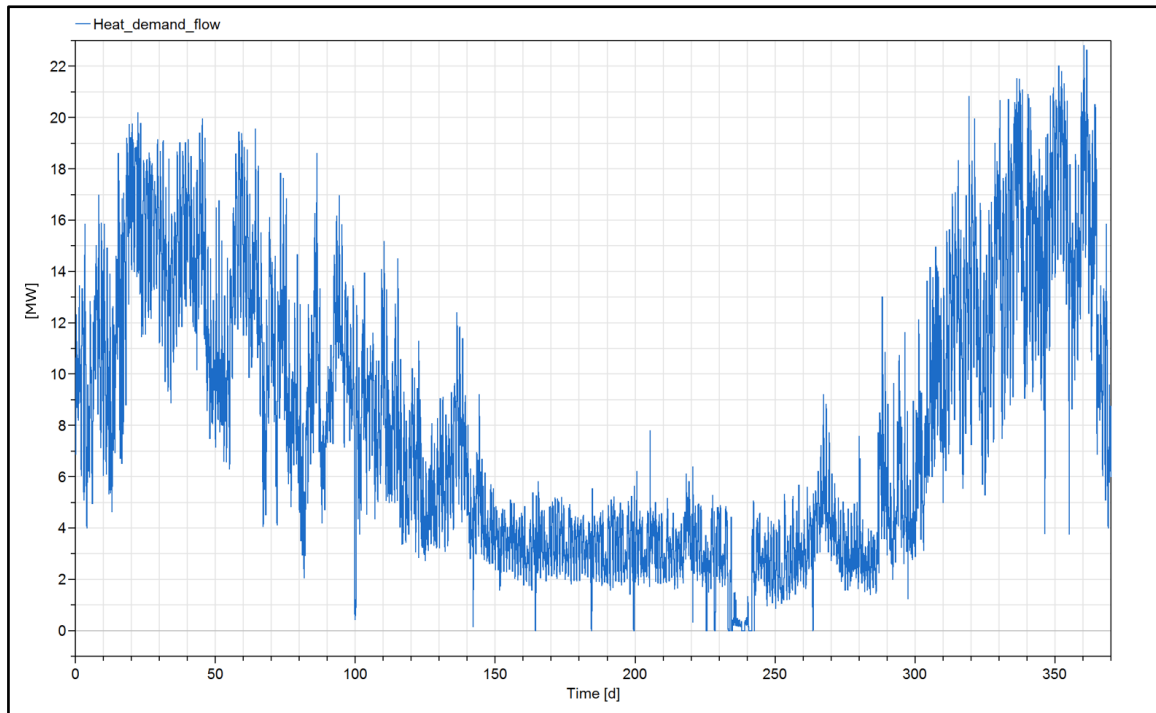


Figure 4.2 Specific hourly energy flow demand profile for 2023

4.2 PTES operating states

This report simulates the operation of the corresponding systems over a 5-year period. It is important to note that although each system employs a different integration strategy, they all rely on the same controller and therefore share identical logical control and feedback mechanisms. Consequently, all integration strategies should exhibit the same PTES operating behavior.

Figure 4.3 illustrates the operating states of the PTES in its fourth year of simulation, while Figure 4.4 employs color-coded markers to indicate the intervals during which the PTES operates in different states. Based on the definition of $\dot{Q}_{discharge}$ provided in Section 3.3.3, the PTES were charging during the summer period (highlighted by the purple and black boxes). The PTES first heats its top segment to the maximum allowable temperature of 90 °C (362 K), a process that requires approximately 170 days. Thereafter, the system transitions into a hybrid heating mode in which both the top and second segments are heated; during this phase, the controller maintains the top segment at its maximum temperature while simultaneously increasing the temperature of the second segment.

During the winter period (highlighted by the orange box), the PTES supplies heat to the DHC network. In this phase, the internal temperature of the PTES decreases rapidly until it reaches the minimum permissible temperature of 60 °C (332 K), at which point the discharging process terminates.

For the remainder of the time, the PTES remains in an idle state. This occurs when the system determines that neither charging nor discharging is required, or when the PTES is unable to perform either operation. This behavior is primarily reflected in two intervals (highlighted by the green boxes). In the first interval, the PTES is unable to supply energy to the DHC network for an extended period because the energy accumulated during the charging phase in the summer of the third year has been fully depleted by the end of that year. This is evidenced by the internal temperature of the PTES approaching or falling below the minimum allowable threshold. During the second interval, the PTES remains in a state where neither charging nor discharge is required. It is noteworthy that, although the top segment temperature of the PTES continues to decrease due to heat losses, the second segment temperature gradually increases. This behavior indicates a delayed thermal response and imperfect temperature stratification, reflecting the certain time required for heat transfer between the two segments.

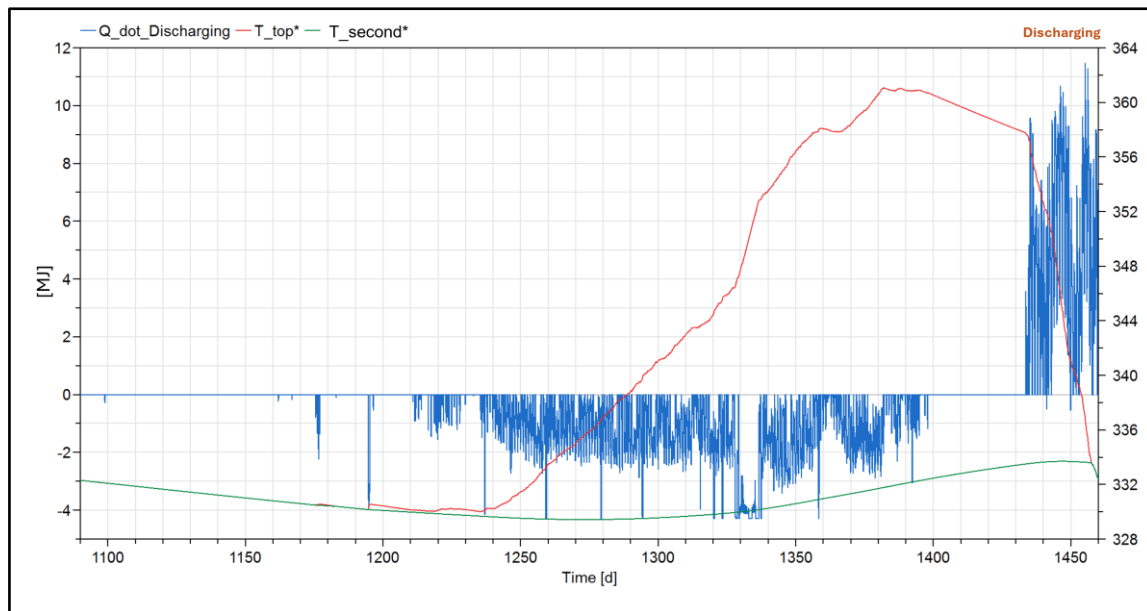


Figure 4.3 Operating states of PTES and situation of PTES internal temperature

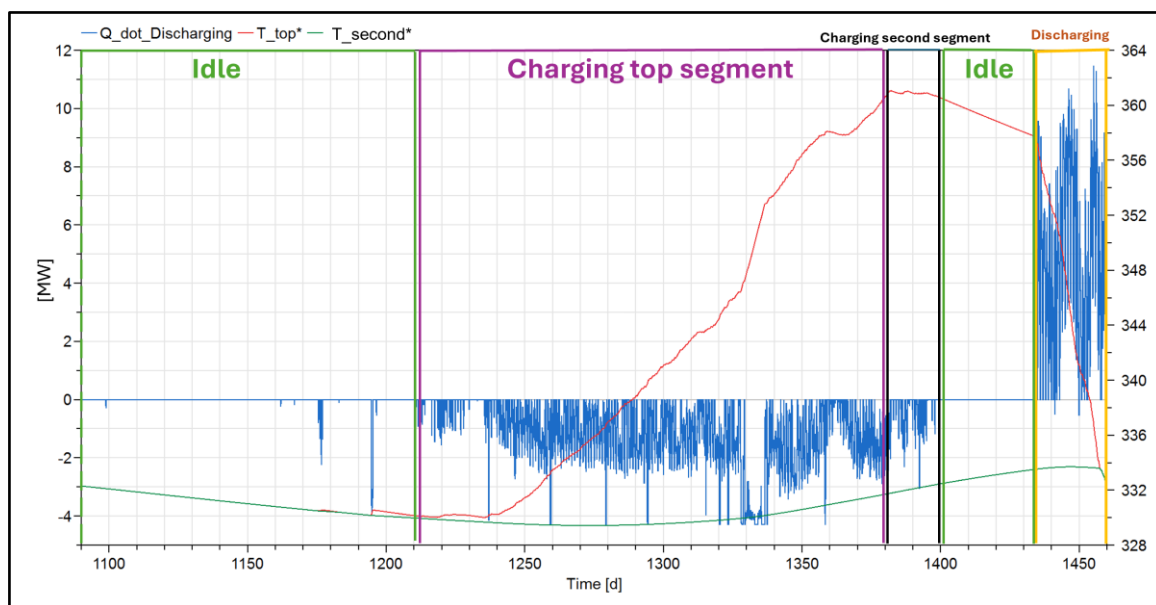


Figure 4.4 Operating states of PTES and situation of PTES internal temperature (With colorful highlighted)

4.3 Integrating strategies performance

To evaluate the performance of the proposed integration strategies, sensitivity analyses are conducted to assess the impact of different temporal resolutions on the simulation results. In this report, DHC1 is used as the reference integration strategy to evaluate the exergy utilization efficiency η_1 of this system under different temporal resolutions (hourly, weekly, monthly, and annual resolutions). As shown in Figure 4.5, the values of η_1 obtained at hourly, weekly, and monthly resolutions are nearly identical. In contrast, the annual resolution yields slightly lower efficiency, with a deviation of approximately one percentage point compared to the other resolutions. Considering both data consistency and the results of the sensitivity analysis, all subsequent simulations in this report are conducted using an hourly temporal resolution.

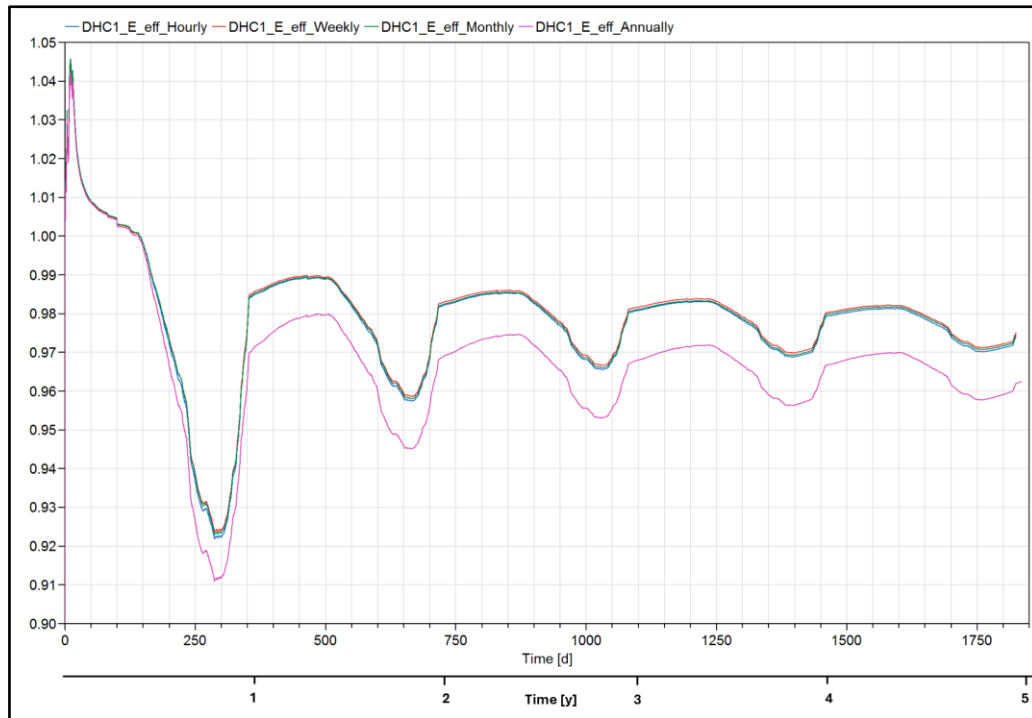


Figure 4.5 Exergy utilization efficiency of DHC1 in several different temporal resolutions

Figure 4.6 presents the exergy utilization efficiency of the two integration strategies, DHC1 and DHC2, together with the control group DHC0. For DHC2, two scenarios are evaluated: one assuming an ideal high-temperature heat pump with a second-law efficiency of 1, and another assuming a realistic high-temperature heat pump with a second-law efficiency of 0.5.

The visualizations illustrate the temporal evolution of the ratio between the two integrals defined in Equations 4 and 6. Over the five-year simulation period, the fluctuations in exergy utilization efficiency associated with each integration strategy gradually diminish. It is therefore reasonable to infer that the exergy utilization efficiency would converge toward a stable value if the simulation were extended over a longer time horizon.

The exergy utilization efficiency of DHC0 remains consistently equal to 1, serving as the baseline case. Owing to the simplified system configuration, which is intended to isolate and highlight the performance of PTES integration within the DHC network, heat losses that are common to all systems are neglected in the simulation.

When comparing the two integration strategies, DHC1 exhibits a substantially higher exergy utilization efficiency η_1 than DHC2, including its idealized configuration. Moreover, when DHC2 is equipped with a realistic high-temperature heat pump, it demonstrates the poorest performance, with an exergy utilization efficiency $\eta_{2,real}$ well below the baseline. Even under the assumption of an ideal high-temperature heat pump, the performance of DHC2 $\eta_{2,ideal}$ still does not reach the level achieved by DHC1.

Table 1 summarizes the exergy utilization efficiency of all integration strategies under the various evaluated conditions. The reported values correspond to the results obtained after a 5-year simulation period.

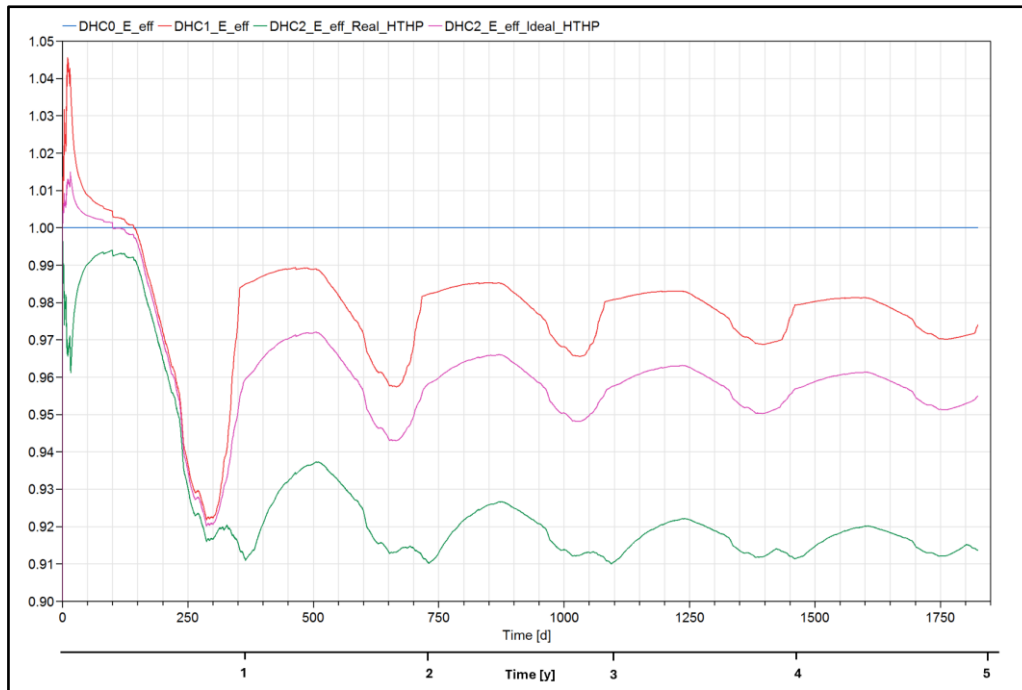


Figure 4.6 Exergy utilization efficiency varying of different integrating strategies with time series

Table 1 Exergy utilization efficiency of different integrating strategies

Type of systems (including all configurations)	Exergy utilization efficiency η
DHC0	1
DHC1	0.974
DHC2 (Real HT-HP)	0.914
DHC2 (Ideal HT-HP)	0.955

Figure 4.7 illustrates the cumulative total exergy consumption of the two integration strategies, DHC1 and DHC2, as well as the control group DHC0 over a five-year simulation period. For DHC2, the total exergy consumption accounts for both the exergy input from the heat source and the electrical power required to drive the high-temperature heat pump. Three distinct curves are shown for DHC2, corresponding to an ideal HT-HP, a realistic HT-HP, and a case considering only the exergy input from the heat source.

The annual exergy consumption exhibits a clear cyclical pattern, with significantly higher demand during the winter period and substantially lower exergy input during the summer period.

When comparing the different integration strategies and their respective configurations, DHC0 exhibits the lowest total exergy consumption, followed by DHC1, while DHC2 shows the highest consumption. Replacing the realistic HT-HP configuration in DHC2 with an idealized heat pump significantly reduces its total exergy consumption; however, it remains higher than that of DHC1. Overall, these results are consistent with the corresponding energy utilization efficiency observed for each system.

It is noteworthy that when considering only the heat source contribution of DHC2, as indicated by the black curve in Figure 4.7, the exergy supplied by the heat source is significantly lower than that of DHC1.

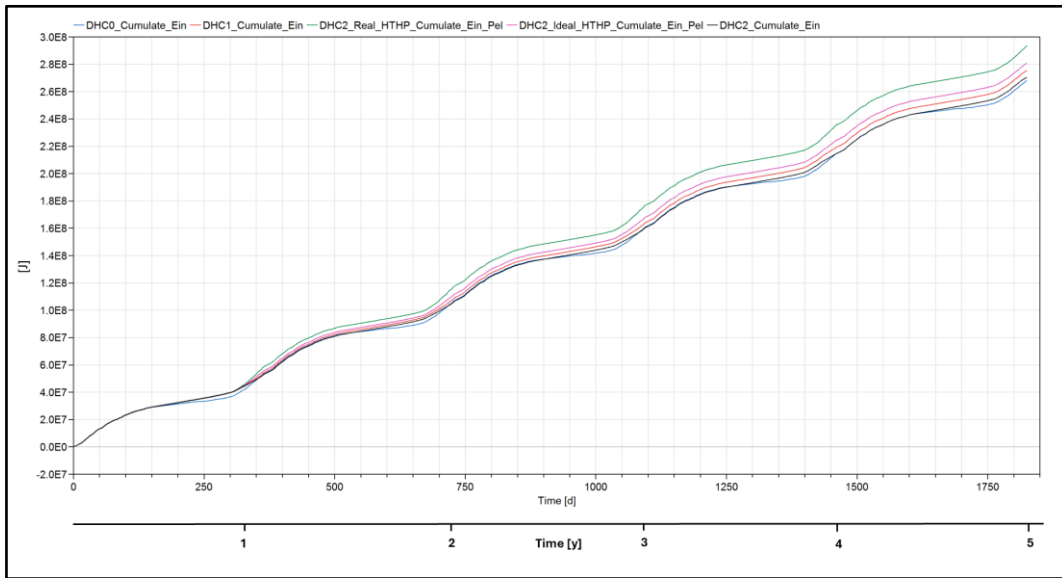


Figure 4.7 Cumulate total exergy consumption of different integrating strategies

Figure 4.8 presents the cumulative total exergy consumption of the two integration strategies in the fifth simulation year. DHC2 is simulated under different configurations.

Table 2 summarizes the corresponding annual total exergy consumption for each case. It should be noted that the annual values reported in Table 2 are derived from the fifth year of simulation rather than from an arithmetic average over the five-year period. This approach is adopted to mitigate the influence of initial-conditioned data anomalies that may occur during the first simulation year.

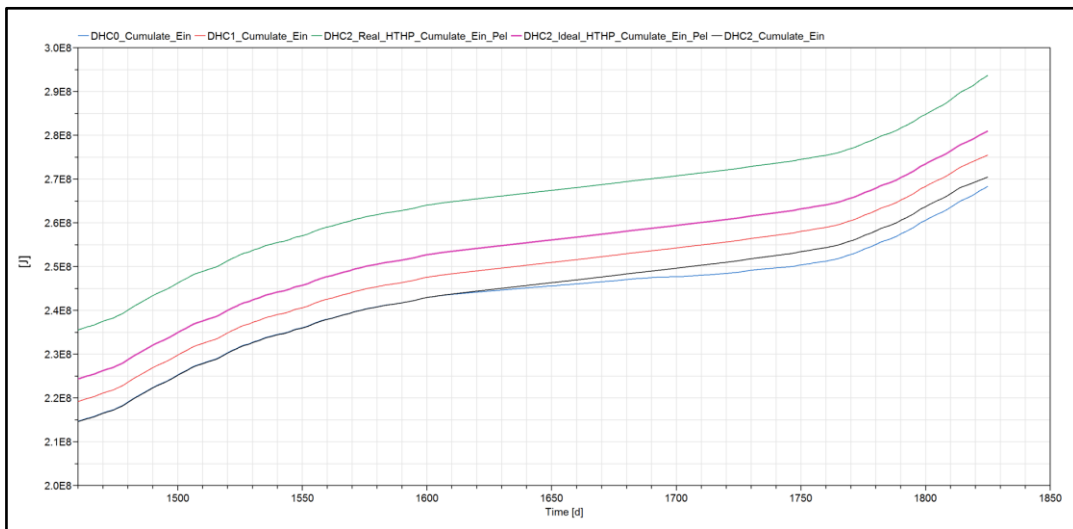


Figure 4.8 Cumulate total exergy consumption of different integrating strategies in fifth year

Table 2 Annually cumulate total exergy consumption of different integrating

Type of System	configurations	Annually exergy consumption [MJ]
DHC0	\dot{E}_{in}	53.66
DHC1	\dot{E}_{in}	56.28
DHC2	$\dot{E}_{in}+P_{el}$ (Real HT-HP)	58.15
DHC2	$\dot{E}_{in}+P_{el}$ (Ideal HT-HP)	56.63
DHC2	\dot{E}_{in}	55.84

5 Discussion of results

The primary objective of this report is to assess the technical feasibility of several potential strategies for integrating PTES components into high-temperature DHC networks by using exergy-based analytical methods. In addition, the report seeks to develop a concise and practical simulation framework that focuses on exergy flow analysis to validate the proposed integration strategies.

After simulations executed, Results demonstrate the potential of PTES to regulate the supply of variable sustainable heat sources. Furthermore, by clearly defining system boundaries and implementing an exergy-based simulation framework, the performance of **DHC system with PTES preheating integration (DHC1)** and **DHC system with PTES back-flow integration (DHC2)** is systematically analyzed.

PTES operating states

Overall, the transitions between the different operating states of the PTES exhibit well-defined boundaries. The charging and discharging states are consistent with the characteristics of the energy flow demand profile used in the simulation: modeling framework successfully captures charging behavior during the summer period and discharging behavior during the winter period. In general, the controller performs as intended.

The internal temperature evolution of the PTES is particularly noteworthy. As indicated by the purple and black highlighted regions in Figure 4.4, the temperature of the top segment increases from 57 °C (330 K) to the maximum value permitted by the controller. Once this maximum temperature is reached, the second segment of the PTES begins to charge. Because the energy supplied to the PTES over the entire charging period is sufficient to raise the top segment temperature T_{top} to the prescribed maximum, the temperature limit defined by the controller can be considered reasonable.

It should be noted that during the phase in which the controller enters the second segment charging mode (black highlighted region), the top segment temperature T_{top} decreases because of intrinsic thermal losses within the PTES. Consequently, this operating state is more accurately characterized as a period in which the top and second segments are alternately reheated rather than a strictly sequential charging process.

As illustrated in Figure 4.4, during the second idle period (highlighted in green), the top segment temperature T_{top} exhibits a decreasing trend, while the second segment temperature T_{2nd} continues to increase. During this interval, the PTES remains idle and does not exchange energy with the DHC network. The reduction in T_{top} is attributed to thermal losses, whereas the increase in T_{2nd} results from delayed heat conduction from the upper segment to the lower segment, reflecting the transient nature of internal heat transfer within the storage.

It is evident that the storage capacity of the PTES is insufficient to provide effective energy regulation over the entire winter period. As indicated by the orange highlighted region in Figure 4.4, the PTES remains in a discharging state for only approximately 25 days. During this phase, the internal temperature of the PTES decreases rapidly until it reaches the minimum temperature threshold defined by the controller. Consequently, the PTES remain in idle state after reaching minimum temperature until the onset of the subsequent summer charging period. Increasing the upper threshold of the energy flow supply \dot{Q}_{up} could potentially alleviate this limitation. In addition, the insufficient discharge duration may partly result from a degree of mismatch between the predefined storage model currently employed and the specific characteristics of system being simulated. Developing a more customizable storage model that more closely reflects the physical and operational conditions described in this report therefore represents a potential avenue for further improvement.

Exergy utilization efficiency

As shown in Figure 4.5, the exergy utilization efficiency of DHC1 is nearly identical when evaluated at hourly, weekly, and monthly temporal resolutions. In contrast, the annual resolution yields an efficiency that is approximately one percentage point reduction than those obtained at the finer time scales. slight reduction can likely be attributed to the use of more temporally uniform temperatures, which introduces a bias in the exergy

factor across the DHC network. Overall, the exergy utilization efficiency exhibits low sensitivity to the chosen temporal resolution.

It is important to emphasize that the exergy utilization efficiency η_0 of the control case DHC0 serves solely as a reference baseline in this report. Because the system boundaries defined in the analysis neglect heat losses that are common to all configurations, the resulting value of $\eta_0 = 1$ does not represent the true exergy utilization efficiency of DHC0, but rather a normalized baseline for comparative evaluation. The exergy utilization efficiencies reported for the various integration strategies and their respective configurations represent their performance relative to the baseline case.

As shown in Figure 4.6, with increasing simulation runtime, the exergy utilization efficiency of each integration strategy transitions from a temporally fluctuating value to a stable steady-state value. This behavior arises from the integral property of Equations 4 and 6.

After five years of simulation, representative results were obtained. Among the evaluated configurations, DHC1 exhibits the best performance, achieving an exergy utilization efficiency of 0.974. This result indicates that DHC1 incurs only minimal exergy losses while effectively fulfilling its primary function of energy peak shifting. DHC2 equipped with realistic HT-HP exhibits the lowest exergy utilization efficiency of 0.914 among the evaluated configurations, indicating that this integration strategy incurs substantially higher additional exergy losses compared to DHC1. Replacing the realistic HT-HP with an idealized HT-HP leads to a significant improvement in the exergy utilization efficiency of DHC2 to 0.955, demonstrating that the electrical power required to drive the heat pump constitutes a major source of exergy consumption in this configuration. Nevertheless, even under the ideal HT-HP assumption, the performance of DHC2 remains inferior to that of DHC1.

Total Exergy consumption

In the five-year period simulation, as illustrated in Figures 4.7 and 4.8, DHC1 exhibits the lowest total exergy consumption, followed by DHC2 equipped with an idealized HT-HP, while DHC2 with realistic HT-HP demonstrates the highest total exergy consumption. These findings are consistent with the corresponding exergy utilization efficiencies, thereby supporting the validity and consistency of the preceding results.

It is worth noting that Figures 4.7 and 4.8 include part of cumulative exergy consumption curves (black lines) for DHC2 that account solely for the contribution from the heat source during operation. When only this heat source input is considered, the exergy consumption of DHC2 is only marginally lower than that of the baseline control group DHC0. This observation indicates that the electrical power required to drive the HT-HP constitutes a substantial portion of the total exergy consumption in the DHC2 configuration.

Summary

Overall, DHC1 offers higher performance than DHC2. This means that the integration strategy can fulfill its primary function of cross-seasonal energy allocation for PTES with less additional exergy supply. DHC2 has lower performance, with power consumption driving HT-HP accounting for a significant portion of the total exergy consumption of the supply system. Improving the second-law efficiency of HT-HP can effectively enhance the performance of DHC2. In certain specific application scenarios, such as those with limited heat source loads or where the grid bears the main supply pressure, or in the context of mature low-carbon electricity, DHC2 may be more competitive than DHC1 because it trades additional exergy for flexibility and system resilience.

6 Conclusions

6.1 Key Findings

The primary objective of this report was to investigate technically feasible strategies for integrating Pit Thermal Energy Storage (PTES) into high-temperature district heating and cooling (DHC) networks, using an exergy-based analytical framework. This report developed an exergetic modeling framework to support subsequent simulations evaluating the performance of the proposed integration strategies. Two integration strategies: **DHC system with PTES preheating integration (DHC1)** and **DHC system with PTES back-flow integration (DHC2)** were evaluated and compared.

The results demonstrate that PTES can effectively achieve seasonal energy peak shifting in DHC systems by charging surplus heat during periods of low demand and discharging it during peak demand periods. The simulation framework successfully captured realistic charging behavior in summer and discharging behavior in winter, confirming the technical feasibility of PTES operation under the defined control logic.

From an exergy perspective, clear performance differences were observed between the integrating strategies. DHC1 achieved the higher exergy utilization efficiency, indicating minimal additional exergy losses while fulfilling its peak-shifting function. In contrast, DHC2 exhibited lower performance, primarily due to the additional electrical exergy required to operate the high-temperature heat pump. DHC2 did not outperform DHC1 even under idealized heat pump conditions.

Overall, the findings confirm that indirect PTES integration via preheating is one of well exergy-efficient strategies for high temperature DHC networks within the investigated system boundaries. Because PTES integration via back-flow requires a lower exergy input from the heat source, this integration strategy may be more competitive in application scenarios characterized by low heat source availability or within energy systems supported by mature low-carbon electricity supplies.

6.2 Limitations

Despite the robustness of the analytical framework, several limitations should be acknowledged.

First, the PTES was represented using an existing stratified storage model from the “Buildings” Library, which does not fully capture the detailed properties of real pit thermal energy storage systems. Consequently, thermal losses and energy storage behavior may differ compared to an actual PTES installation.

Second, heat losses within the district heating network and related components were intentionally excluded from the system boundaries to allow for a clear comparison of integration strategies. While this approach is suitable for relative performance assessment, it results in an idealized DHC network and does not represent the realistic exergy efficiency of real DHC networks.

Third, the control strategy and PTES model were predefined and not optimized. The limited discharge duration during winter period indicates that the selected setting and parameters may not be sufficient to fully cover seasonal demand, potentially underestimating the achievable benefits of PTES integration.

Finally, the high-temperature heat pump used in DHC2 was modeled using simplified assumptions regarding its coefficient of performance and second-law efficiency. Real performance may vary depending on operating conditions, technological maturity, and integration with the electricity grid.

6.3 Recommendation

This report has largely achieved its intended objectives with several inherent limitations indicate opportunities for further work.

From the perspective of exergy analysis, the system boundaries could be redefined to place greater emphasis on overall system efficiency. From the perspective of modeling refinement, more detailed PTES representations could be developed by incorporating site-specific geometries, soil thermal properties, and liner aging effects, thereby enabling more accurate simulations of long-term energy storage behavior. Furthermore, employing a more realistic HT-HP model would contribute to improving the overall accuracy of the simulation framework.

Optimizing the existing control logic also represents a promising area for improvement, as more efficient control strategies could better exploit the potential benefits of PTES integration.

Future research could focus on evaluating a broader range of potential integrating strategies based on the analytical framework established in this report and existing references, thereby expanding the scope of feasible high-temperature DHC integration concepts. In addition, assessing the feasibility of PTES integration with high-temperature DHC systems under practical, real-world conditions and designing application represents an important direction for further investigation.

Furthermore, it is essential to complement integration strategy assessments with cross-sectoral evaluations, such as cost-effectiveness and environmental impact analyses. This research aims to provide a more comprehensive basis for investment and policy deciding usefully.

7 References

Bolton, R., Cameron, L., Kerr, N., Winkler, M., & Desguers, T. (2023). Seasonal thermal energy storage as a complementary technology: Case study insights from Denmark and The Netherlands. *Journal of Energy Storage*, 73(D), 109249. <https://doi.org/10.1016/j.est.2023.109249>

Bundesamt für Meteorologie und Klimatologie MeteoSchweiz (2025). Bodenmessdaten und homogene Messreihen der einzelnen Stationen mit erläuternden Metadaten. <https://www.meteoschweiz.admin.ch/service-und-publikationen/applikationen/ext/daten-ohne-programmierkenntnisse-herunterladen.html#lang=de&mdt=normal&pgid=&sid=&col=&di=&tr=&hdr=>

Bundesamt für Statistik (Federal Statistical Office) (2023). Gebäude- und Wohnungsstatistik 2023. <https://www.bfs.admin.ch/bfs/de/home/aktuell/medienmitteilungen.gnpdetail.2024-0526.html>

Chambers, J., Narula, K., Sulzer, M., & Patel, M. K. (2019). Mapping district heating potential under evolving thermal demand scenarios and technologies: A case study for Switzerland. *Energy*, 176(1), 682-692. <https://doi.org/10.1016/j.energy.2019.04.044>

Dahash, A., Ochs, F., Janetti, M. B., & Streicher, W. (2019). Advances in seasonal thermal energy storage for solar district heating applications: A critical review on large-scale hot-water tank and pit thermal energy storage systems. *Applied Energy*, 239(1), 296-315. <https://doi.org/10.1016/j.apenergy.2019.01.189>

Dahash, A., Steingrube, A., Elci, M., (2017). A Power-Based Model of a Heating Station for District Heating (DH) System Applications. 12th International Modelica Conference, 12. https://www.researchgate.net/publication/316877537_A_Power-Based_Model_of_a_Heating_Station_for_District_Heating_DH_System_Applications

Dincer, I., & Cengel, Y. A. (2001). Energy, entropy and exergy concepts and their roles in thermal engineering. *Entropy*, 3(3), 116-149. <https://doi.org/10.3390/e3030116>

Eight Advisory (2025). Heating Up Navigating Growth Barriers in Swiss District Heating. https://www.8-international.com/wp-content/uploads/2025/07/Heating-Up_-_Navigating-growth-barriers-in-Swiss-district-heating.pdf

Epp, B. (2020, Oct 27) Improved design for giga-size pit heat storage. Solarthermalworld.org. <https://solarthermalworld.org/news/improved-design-giga-size-pit-heat-storage/>

Gao, M., Fan, J., Furbo, S., Wang, D., & Liu, Y. (2023). Thermal performance analysis of a large-scale water pit heat storage. *Proceedings of the International Conference on Evolving Cities*, 9–16. <https://doi.org/10.55066/proc-iccc.2022.116>

Gong, M., & Werner, S. (2015). Exergy analysis of network temperature levels in Swedish and Danish district heating systems. *Renewable Energy*, 84(1), 106-113. <https://doi.org/10.1016/j.renene.2015.06.001>

Jangsten, M., Kensby, J., Dalenbäck, J.-O., & Trüschel, A. (2017). Survey of radiator temperatures in buildings supplied by district heating. *Energy*, 137(1), 292-301. <https://doi.org/10.1016/j.energy.2017.07.017>

Johansen, K., & Werner, S. (2022). Something is sustainable in the state of Denmark: A review of the Danish district heating sector. *Renewable and Sustainable Energy Reviews*, 158(1), 112117. <https://doi.org/10.1016/j.rser.2022.112117>

Keenan J.H. (1941), *Thermodynamics*, 3rd ed., John Wiley And Sons,inc,ny.

- Lund, H., Werner, S., Wiltshire, R., Svendsen, S., Thorsen, J. E., Hvelplund, F., & Mathiesen, B. V. (2014). 4th Generation District Heating (4GDH): Integrating smart thermal grids into future sustainable energy systems. *Energy*, 68(1), 1-11. <https://doi.org/10.1016/j.energy.2014.02.089>
- Munčan, V., Mujan, I., Macura, D., Anđelković, A. S., (2024). The state of district heating and cooling in Europe - A literature-based assessment. *Energy*, 304 30. <https://doi.org/10.1016/j.energy.2024.132191>
- Pons, M. (2009). On the reference state for exergy when ambient temperature fluctuates. *International Journal of Thermodynamics*, 12(3), 161–170. <https://doi.org/10.5541/ijot.246>
- Sifnaios, I., Fan, J., & Jensen, A. R. (2025). Integration of pit thermal energy storages into district heating networks – a techno-economic case study. *Applied Thermal Engineering*, 279(D), 127770. <https://doi.org/10.1016/j.applthermaleng.2025.127770>
- Sifnaios, I., & Jensen, A. R. (2023). Experiences from the first short-term pit thermal energy storage. In *Proceedings of the Solar World Conference 2023 International Solar Energy Society*. <https://doi.org/10.18086/swc.2023.04.12>
- Sveinbjörnsson, D., Jensen, L. L., Trier, D., Bava, F., Ben Hassine, I., & Jobard, X. (2019). D2.3 - Large storage systems for DHC networks. PlanEnergi & HFT Stuttgart. <https://ec.europa.eu/research/participants/documents/downloadPublic?documentIds=080166e5c2089739&appId=PPGMS>
- Torío, H., & Schmidt, D. (2010). Development of system concepts for improving the performance of a waste heat district heating network with exergy analysis. *Energy and Buildings*, 42(10), 1601-1609. <https://doi.org/10.1016/j.enbuild.2010.04.002>
- Wall, G., & Gong, M. (2001). On exergy and sustainable development—Part 1: Conditions and concepts. *Exergy, An International Journal*, 1(3), 128-145. [https://doi.org/10.1016/S1164-0235\(01\)00020-6](https://doi.org/10.1016/S1164-0235(01)00020-6)
- Xiang, Y., Xie, Z., Furbo, S., Wang, D., Gao, M., & Fan, J. (2022). A comprehensive review on pit thermal energy storage: Technical elements, numerical approaches and recent applications. *Journal of Energy Storage*, 55(C), 105716. <https://doi.org/10.1016/j.est.2022.105716>

Appendix

A. Detailed schematic of system boundaries for different DHC systems

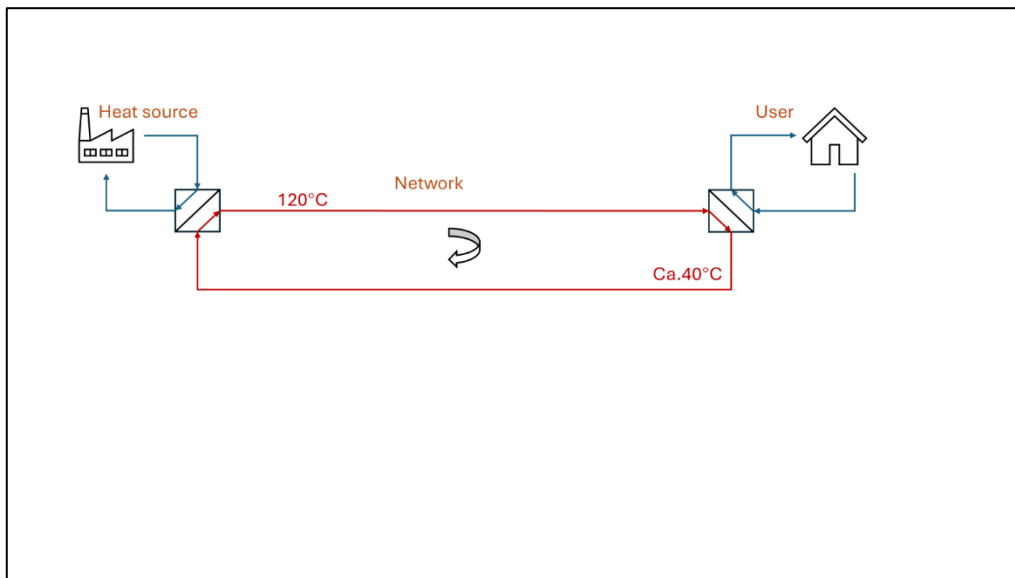


Figure A1 The entrie system of DHC0 without system boundary

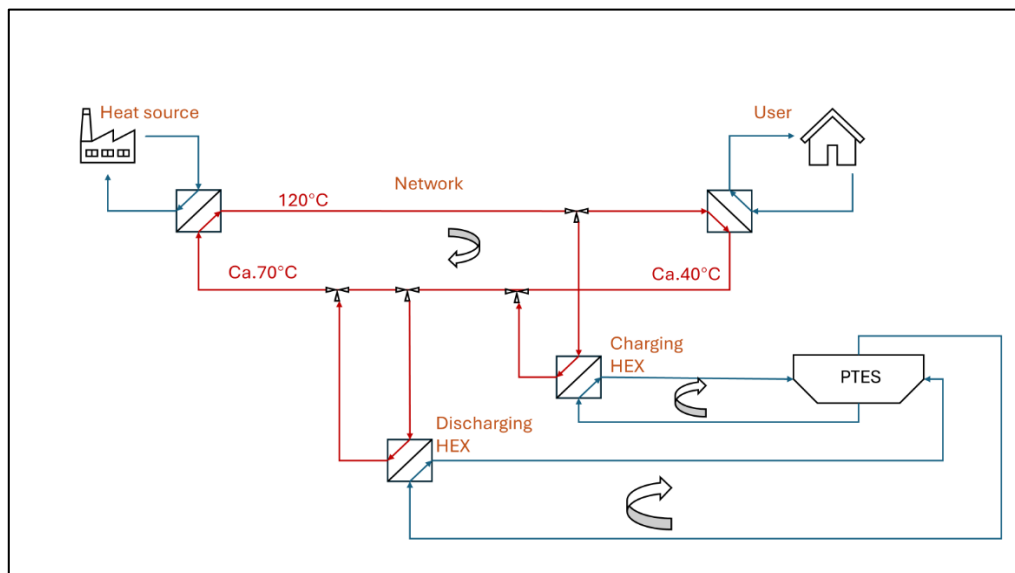


Figure A2 The entrie system of DHC2 without system boundary

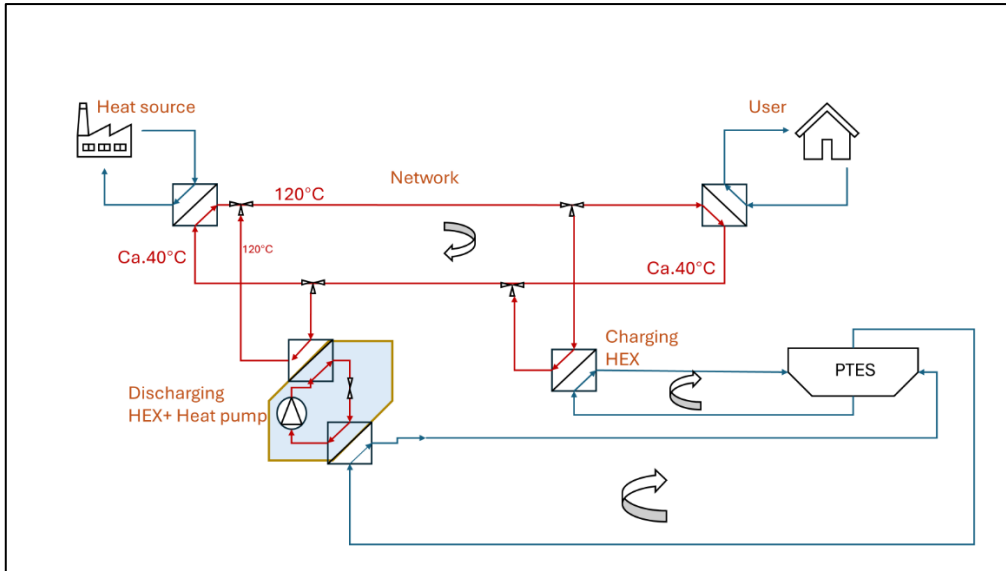


Figure A3 The entrie system of DHC2 without system boundary

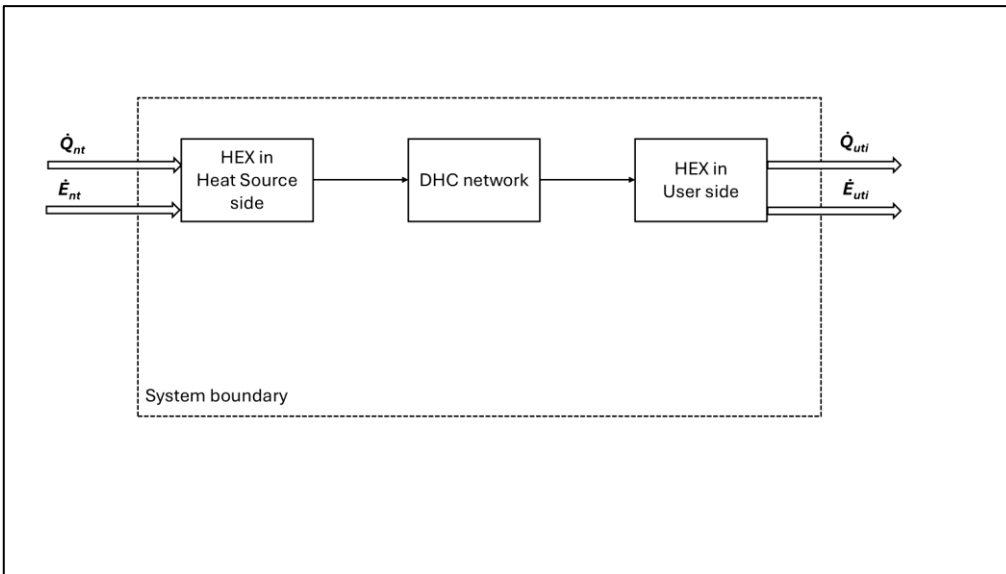


Figure A4 The black boxes of DHC0 with system boundary

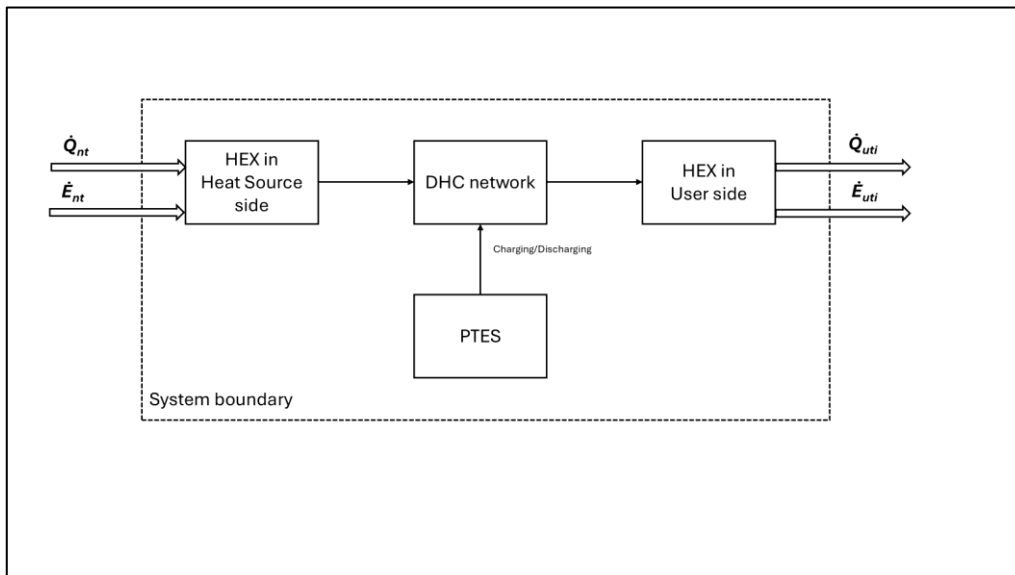


Figure A5 The black boxes of DHC1 with system boundary

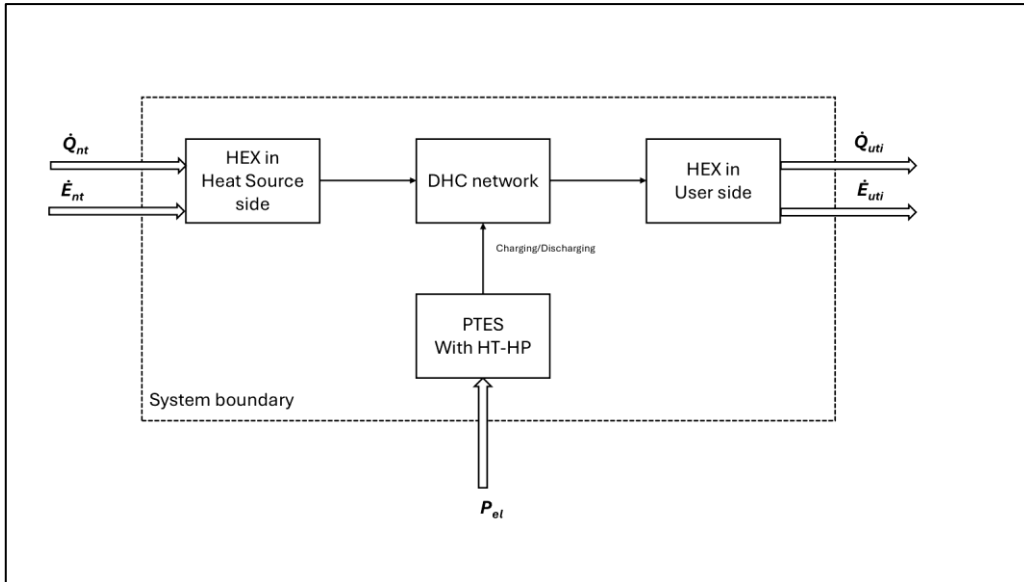


Figure A6 The black boxes of DHC2 with system boundary

B. Detailed information regarding Dymola modeling

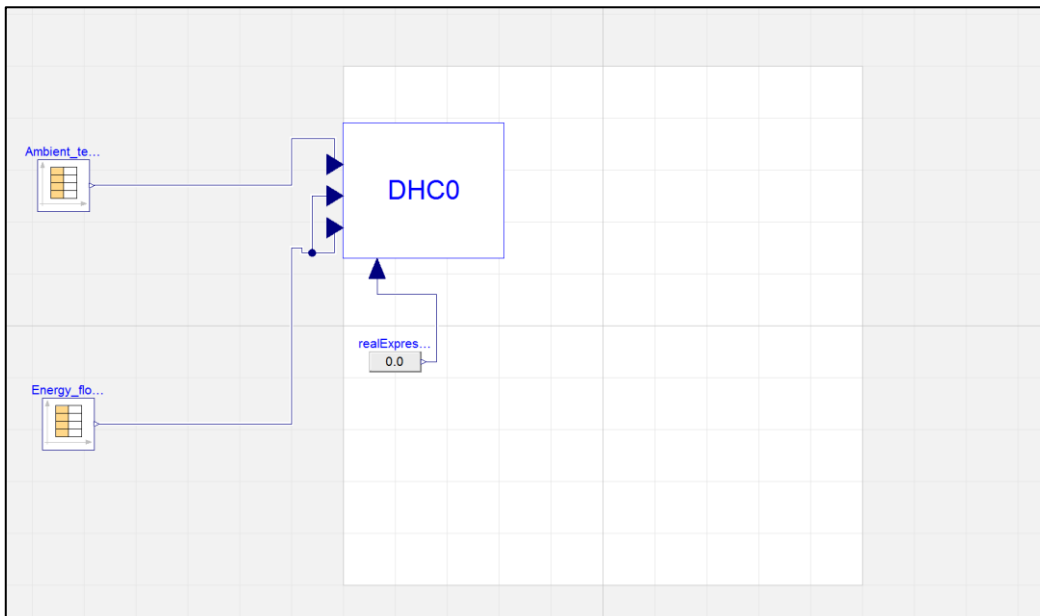


Figure B1 The top layer modeling of DHC0

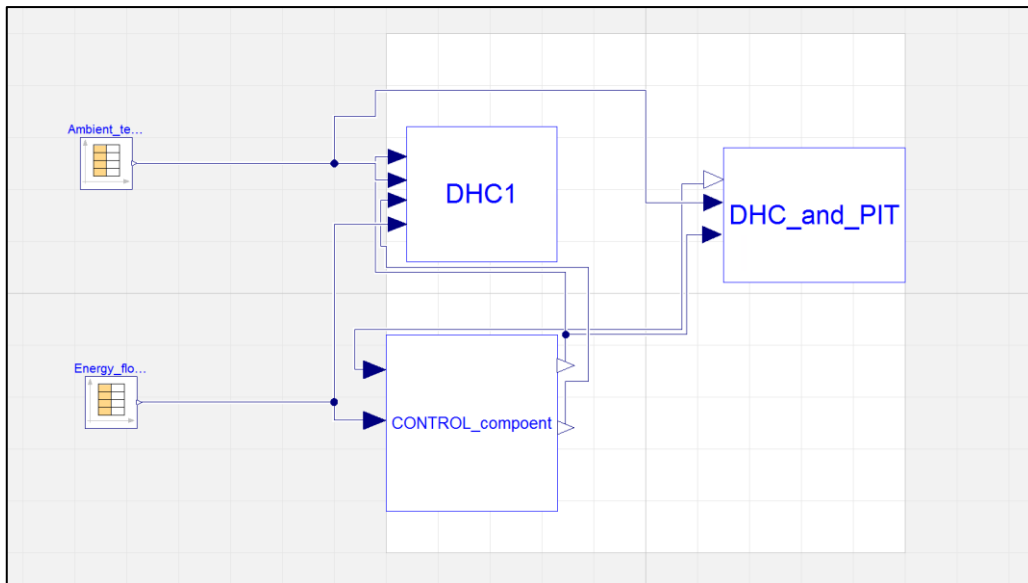


Figure B2 The top layer modeling of DHC1

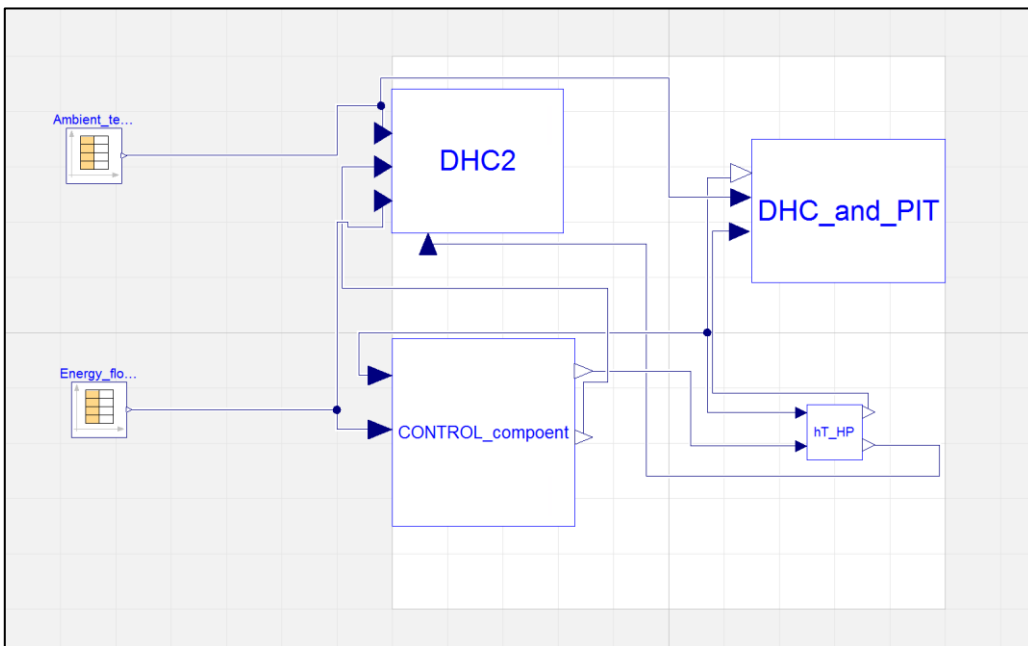


Figure B3 The top layer modeling of DHC2

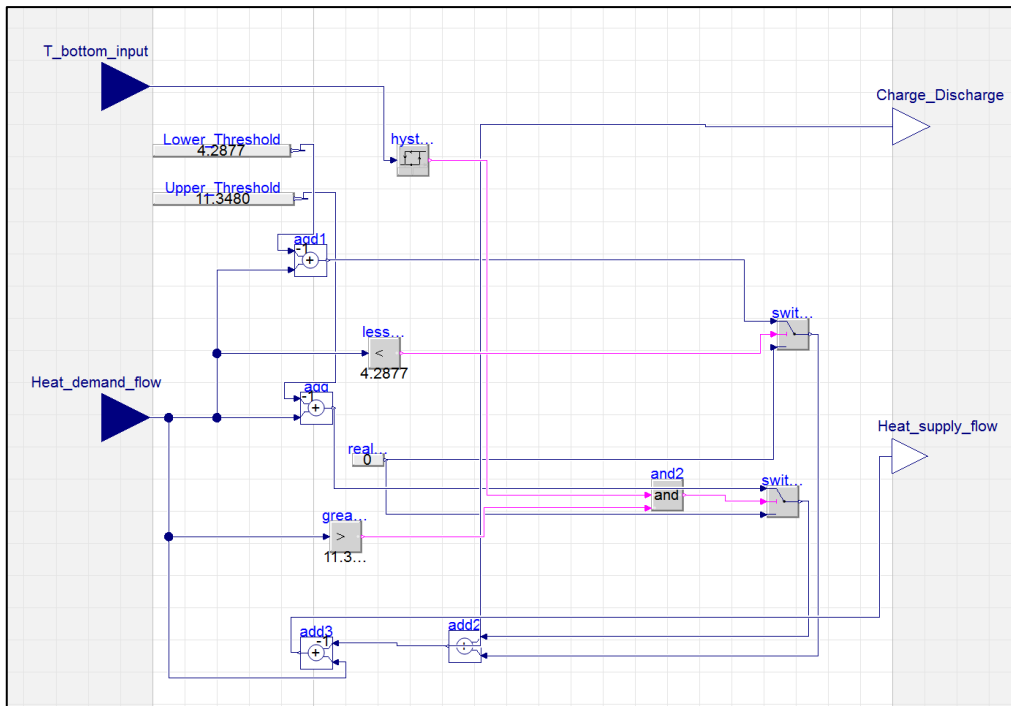


Figure B4 The logic controller component modeling

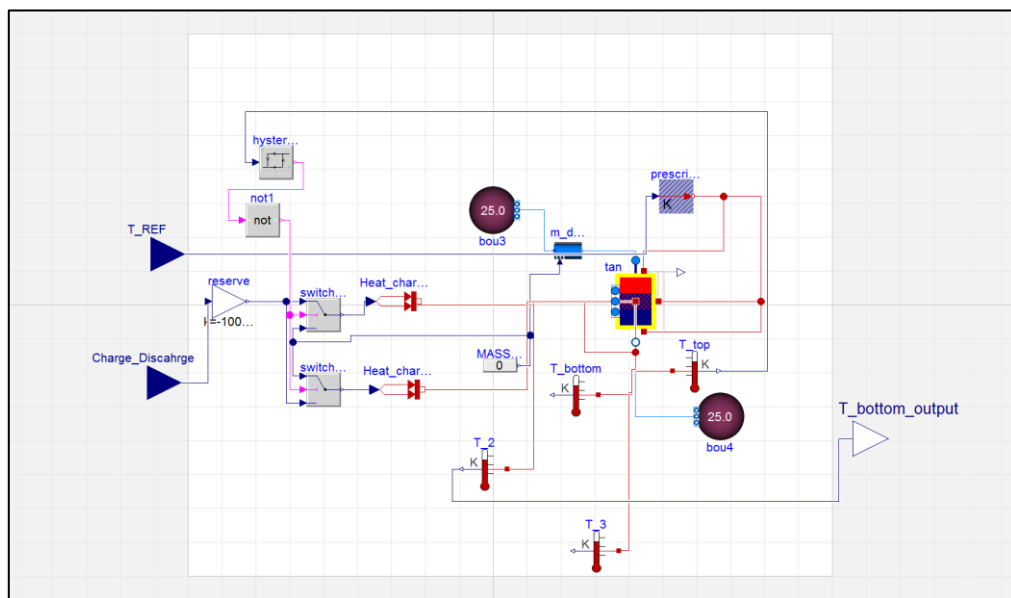


Figure B5 the PTES component modeling

```

model HT_HP
    Real es;
    Real ec;
    Real COP;
equation
    es=1;
    if Qcd<0 then
        Pel=0;
        ec=ec;
        COP=COP;
        Qcd_fix=Qcd;
    else
        ec=(125+273.15)/((125+273.15)-(Tb-5));
        COP=es*ec;
        Pel=Qcd/COP;
        Qcd_fix=Qcd-Pel;
    end if;
end HT_HP;
    
```

Figure B6 The HT-HP component modeling

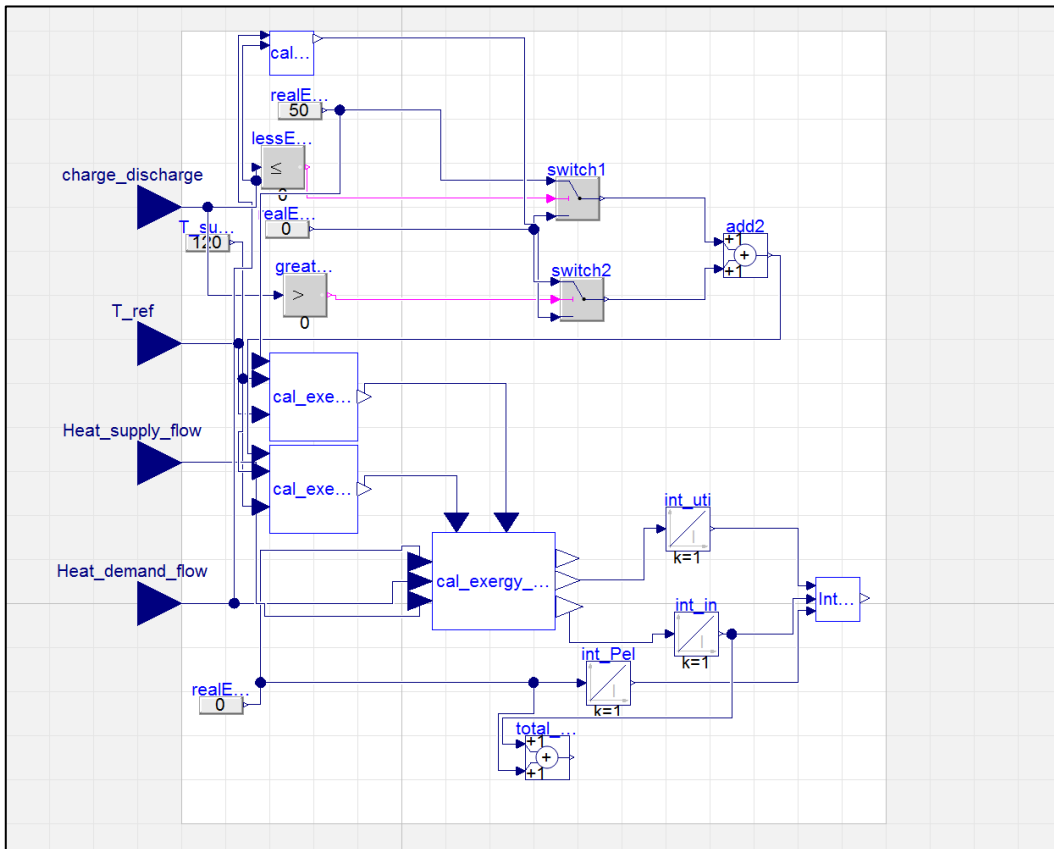


Figure B7 The calculation component of DHC1 modeling

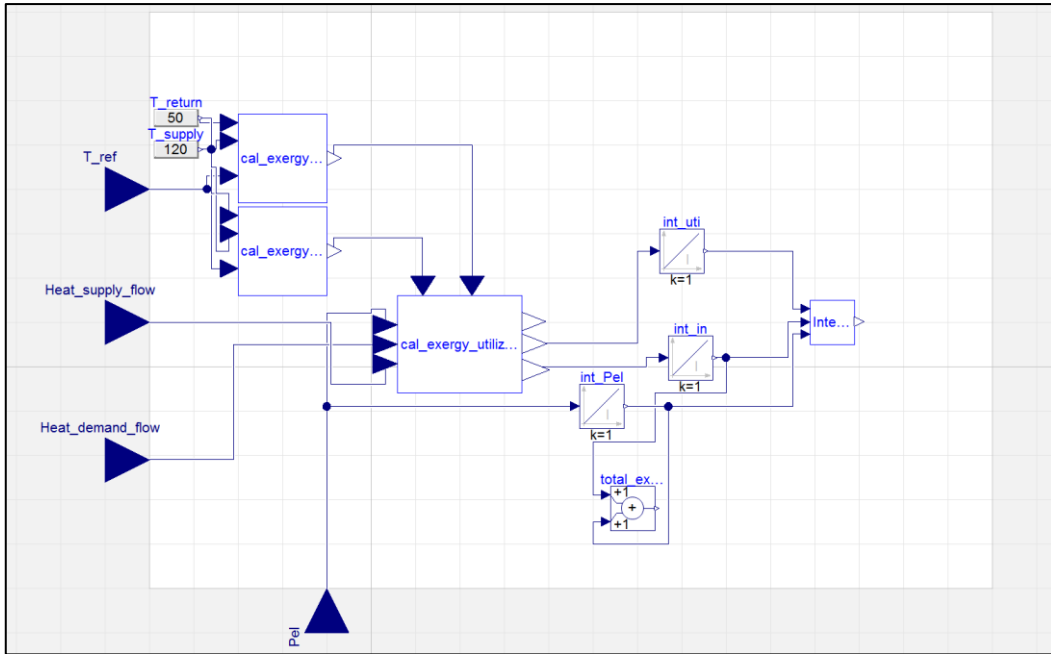


Figure B8 The calculation component of DHC2 modeling

C. Declaration of the use of AI-based tools

Table. C1 documents the use of artificial intelligence in academic work.

Table. C1 Artificial intelligence using

AI based tool	Use case	Scope
Chat-GPT 5.0	Grammar correction, expression standardization	Entire work
Chat-GPT 5.0	Learning Modelica coding	Related parts “Calculating component” and “HT-HP” in Dymola software